

# Aqueous-organic and aqueous-vapor interfacial phenomena for three phase systems containing CO<sub>2</sub>, CH<sub>4</sub>, n-butanol, n-dodecane and H<sub>2</sub>O at saturation conditions

R. Villablanca-Ahues<sup>a,\*</sup>, R. Nagl<sup>b</sup>, T. Zeiner<sup>b,c</sup>, P. Jaeger<sup>a</sup>

<sup>a</sup> Institute of Subsurface Energy Systems, Clausthal University of Technology, Clausthal-Zellerfeld, Germany

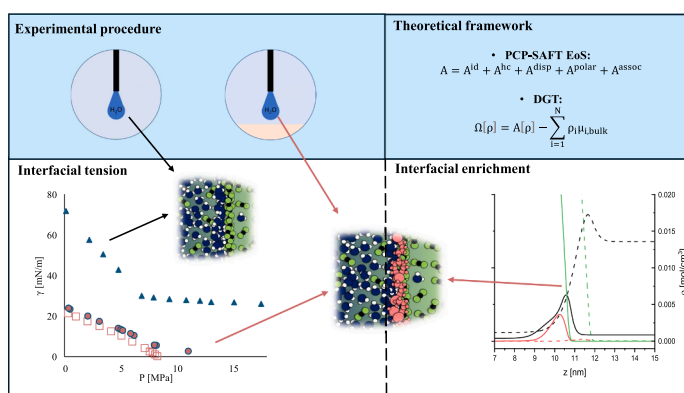
<sup>b</sup> Process Systems Engineering, Graz University of Technology, Graz, Austria

<sup>c</sup> Institute of Thermal Process Engineering, Karlsruhe Institute of Technology, Karlsruhe, Germany

## HIGHLIGHTS

- Predicted & measured IFT and density.
- Competitive- and co-adsorption are observed.
- Interfacial behavior was theoretically predicted and experimentally validated.
- Interfacial tensions are well estimated by the framework based on binary interactions parameters.
- Competitive adsorption, as well as co-adsorption is observed.

## GRAPHICAL ABSTRACT



## ARTICLE INFO

### Keywords:

Interfacial tension  
Phase equilibria  
Ternary systems  
DGT  
PCP-SAFT

## ABSTRACT

A fundamental understanding of the interfacial properties at elevated pressure is essential for processes in the context of the energy transition, such as the storage of CO<sub>2</sub>, H<sub>2</sub> or CH<sub>4</sub>. Systems in such processes have traces of impurities. This work aims to systematically investigate these multi-component systems through simplified vapor-liquid-liquid systems comprising H<sub>2</sub>O, (n-butanol or n-dodecane), and (CO<sub>2</sub> or CH<sub>4</sub>). The model systems are theoretically investigated using the density gradient theory and the PCP-SAFT. The interfacial tension and saturated phase density of the model systems are experimentally measured by the pendant drop and the oscillating tube method, respectively. Good agreement between the theoretical and experimental results is found. It was found that the pure and binary systems of these mixtures can be described well by the introduced model, delivering high quality predictions.

\* Corresponding author.

E-mail addresses: [rafael.villablanca@tu-clausthal.de](mailto:rafael.villablanca@tu-clausthal.de), [rafael.villablanca.14@gmail.com](mailto:rafael.villablanca.14@gmail.com) (R. Villablanca-Ahues).

**Table 1**  
Previous studies on the Interfacial tension of relevant ternary systems.

| Author                      | System  | Technique                                  | T K           | P MPa |
|-----------------------------|---|--|---------------|-------|
| Choudhary et al. [24]       | CO <sub>2</sub> +n-alkane (C <sub>7</sub> -C <sub>19</sub> )<br>CH <sub>4</sub> +n-alkane (C <sub>7</sub> -C <sub>19</sub> )<br>(CH <sub>4</sub> , CO <sub>2</sub> ) +n-alkane (C <sub>7</sub> -C <sub>19</sub> ) | Simulation: Molecular Dynamics; PR EoS+DGT | –             | –     |
| Bing Liu et al. [25]        | CO <sub>2</sub> +H <sub>2</sub> O+oil   | M.S.                                       | –             | –     |
| Georgiadis et al. [16]      | CO <sub>2</sub> +H <sub>2</sub> O+n-decane  | PDM  | <443          | <50   |
| Sohaib Mohammed et al. [2]  | CO <sub>2</sub> +brine+crude oil  | MDS.                                       |               |       |
| Bahramian et al. [4]        | CH <sub>4</sub> +n-decane+H <sub>2</sub> O  | PDM  | 423.15 K      | <28.1 |
| Masamichi Koderá et al. [6] | CH <sub>4</sub> +n-decane+H <sub>2</sub> O  | PDM  | 556.15–571.15 | <10   |
| Cartes M. et al. [26]       | H <sub>2</sub> O+n-hexane + (ethanol or n-butanol) and<br>H <sub>2</sub> O+MTBE + (ethanol or n-butanol)  | PDM  | 329–349       | 0.1   |

**Table 2**  
Chemical specification according to the provider.

| Substances     | Chemical formula                 | Source                           | Purity   | Quality     | CAS       |
|----------------|----------------------------------|----------------------------------|----------|-------------|-----------|
| n-butanol      | C <sub>4</sub> H <sub>10</sub> O | Acros Organics                   | 99.5 %   | Analysis    | 71–36–3   |
| n-dodecane     | C <sub>12</sub> H <sub>26</sub>  | Acros Organics                   | ≥99 %    | Reagent     | 112–40–3  |
| Water          | H <sub>2</sub> O                 | Honeywell/<br>Riedel-de<br>Haen™ |          | HPLC degree | 7732–18–5 |
| Methane        | CH <sub>4</sub>                  | Westfalen                        | 99.995 % |             | 74–82–8   |
| Carbon dioxide | CO <sub>2</sub>                  | Westfalen                        | 99.999 % |             | 124–38–9  |

## 1. Introduction

In the context of assuring a constant future supply of energy, its conversion and storage is becoming a key challenge. Different energy sources are competing for storage capacities in the subsurface where several phases and multiple components coexist at elevated pressures and temperatures, resulting in specific mixture phase and interfacial properties. In conjunction with solid surfaces, these properties result in specific wetting and capillary effects [1] that strongly influence the flow and storage mechanisms of fluids in subsurface porous materials. To understand these multiphase systems, it is necessary to describe and further predict the behavior of the fluid phases at elevated pressure, particularly the phase equilibria, interfacial tension ( $\gamma$ ), and mixture densities ( $\bar{\rho}_i$ ). Therefore, it is crucial to develop and improve existing theoretical models and conduct experiments on representative systems that can capture the effects dominating the phase and interfacial behavior. The representative systems, also known as model systems, must be strategically chosen and systematically studied, gradually increasing their complexity, revealing the change in behavior as components are added.

Before presenting the relevant literature, a clarification regarding the nomenclature used here needs to be made. Previous literature has not always been consistent when referring to the number of phases and components within an inhomogeneous system [2,3]. In this work in particular, the number of phases will be referred to using ordinal numbers, i.e., “binary” and “ternary”, whereas the number of components is denoted using cardinal numbers, i.e., “one”, “two”, “three”, etc.

Some studies have been conducted on the interfacial tension of systems containing several components and phases in the framework of hydrocarbon-reservoir systems [4,5]. However, systematic studies covering the interfacial behavior of systems up to four components in the presence of a compressible phase at enhanced pressures are scarce. Studying a three-component system, Koderá et al. [6] reported the decane+H<sub>2</sub>O interfacial tension and the effect of CH<sub>4</sub> at saturation conditions between 283.2 and 298.2 K, up to 10 MPa. They found a rather weak influence of temperature on the interfacial tension, and a decrease up to 2 MPa, pressure beyond which no further pressure

influence on the interfacial tension is found. Monje-Galvan et al. [7] studied the influence of butanol isomers on the H<sub>2</sub>O+Cyclohexane interfacial tension, describing the surface-active behavior of the isomers at the interface of polar+nonpolar systems. A summary of previous experimental and theoretical studies on the interfacial tension of relevant ternary systems can be seen in Table 1.

Concerning theoretical studies of the interfacial behavior of fluid systems, Stephan et al. studied the interfacial properties of binary systems comprising CO<sub>2</sub>, N<sub>2</sub>, and toluene [8] as well as the CO<sub>2</sub>+cyclohexane system [9]. They found that CO<sub>2</sub> is enriched at the toluene and cyclohexane interfaces, whereas N<sub>2</sub> is also enriched at the toluene interface. The adsorption of CO<sub>2</sub> increases as temperature decreases, and with increasing pressure, up to a maximum, beyond which it decreases to zero around the CO<sub>2</sub>'s critical pressure. Llovell et al. [10] reported the interfacial behavior of vapor-liquid systems comprising several n-alkanes (C<sub>5</sub>-C<sub>14</sub>), CH<sub>4</sub>, CO<sub>2</sub>, and H<sub>2</sub>O observing that CH<sub>4</sub> and CO<sub>2</sub> are absorbed at the n-alkane interfaces. This adsorption becomes stronger as the n-alkane length increases. Lafitte et al. [11] studied the interfacial behavior of the H<sub>2</sub>O+CO<sub>2</sub> system, finding that H<sub>2</sub>O does not enrich at the interface, whereas CO<sub>2</sub> does enrich at the interface. This behavior was also observed in the CH<sub>4</sub>+H<sub>2</sub>O system [12]. Niño-Amezquita et al. [13], agreeing with the findings of Lafitte, found that the CO<sub>2</sub> interfacial enrichment in the H<sub>2</sub>O+CO<sub>2</sub> system decreases at elevated pressures, disappearing at around 39 MPa at 308.2 K.

Based on the associating characteristics of alcohols, alkanes, and H<sub>2</sub>O, Enders and Kahl studied the interfacial behavior of H<sub>2</sub>O+ethanol and H<sub>2</sub>O+n-butanol [14], describing also in a later work the interfacial behavior of alcohol+alkane systems [15]. They observed that alcohols are adsorbed at the vapor-aqueous interface, and that at low alcohol concentrations the enrichment is stronger, whereas at high concentrations, no enrichment is observed. It was found that n-butanol acts as a potential surface active component even at very low concentrations, decreasing the H<sub>2</sub>O-air interfacial tension. Surprisingly, no enrichment of n-butanol was theoretically found at the n-butanol+H<sub>2</sub>O interface. Regarding the interfacial behavior of alcohol+alkane systems, no enrichment of any of the components was observed at the interface.

Most previous interfacial studies on three component systems are conducted in two phase systems, away from the phase equilibrium conditions [16–18]. This approach excludes the interfacial tension of the two other interfaces present at phase equilibrium conditions. Based on a NIST literature report, only one study has been found referring to two components vapor-liquid interfacial behavior of self-, cross-, and non-associating components under typical underground reservoir conditions [19]. This work comprises H<sub>2</sub>O, n-butanol, or n-dodecane in presence of CO<sub>2</sub> or CH<sub>4</sub>.

Considering the available literature, this work focuses on studying the interfacial behavior of ternary systems comprising H<sub>2</sub>O, n-butanol or n-dodecane, and CO<sub>2</sub> or CH<sub>4</sub> at phase equilibrium conditions. The interfacial tension of the aqueous-vapor and aqueous-organic interfaces are studied at 313.15 and 353.15 K, up to 30 MPa. The saturated phase density of the CO<sub>2</sub>-containing system was measured at 313.15 and 333.15 K up to the organic-vapor miscibility pressure. The phase

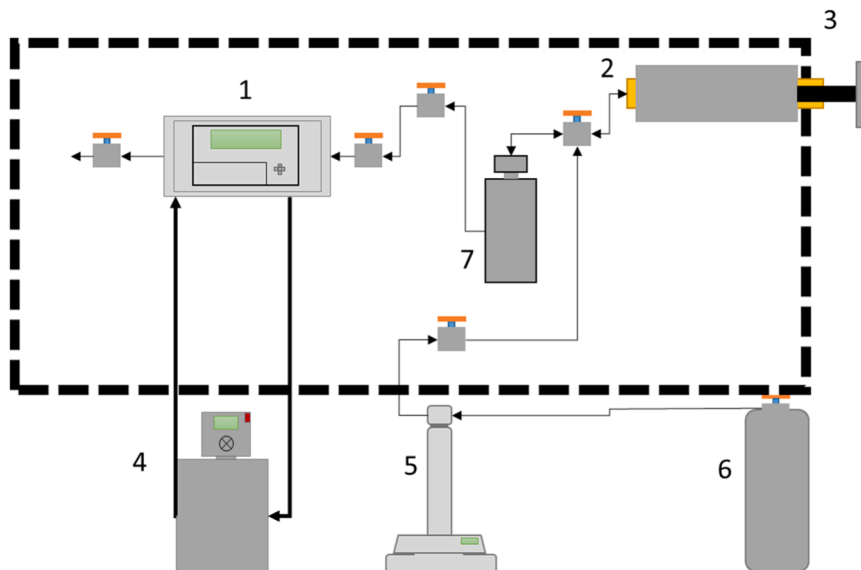


Fig. 1. Experimental set up for measuring densities of gas-liquid systems at equilibrium. Anton Paar density meter (1); Handpump (2); Air Heated Oven (3); Thermostat (4); Automatic Syringe Pump (5); Gas cylinder (6); High pressure equilibration vessel (7).

equilibria and interfacial behavior of the model systems are theoretically predicted by the combination of the density gradient theory (DGT) with the perturbed chain polar statistical associating fluid theory (PCP-SAFT) equation of state given its previous success in describing binary-two components subsystems [13,20–23].

## 2. Materials and methods

### 2.1. Fluids

The fluids in this work are listed in Table 2 and were used as received, i.e., without any further purification.

### 2.2. Density

The setup used to experimentally determine the density of the saturated ternary systems is depicted in Fig. 1. It consists of a saturation vessel (80 mL app) connected to a DMA HPM density meter (Anton Paar, Austria, 0–3 g/cm<sup>3</sup> [3]; 0–140 MPa; 263.15–473.15 K) in combination with a mPDS 2000 v3 display and a pressure transmitter ABB (model 2600 T; ±0.01 bar). The measurements on ternary systems were only carried out for those comprising CO<sub>2</sub>. In the case of CH<sub>4</sub>, influence of water in the vapor phase was neglected, only taking into account the influence of n-dodecane and butanol, known from the measurements on the binary subsystems.

This equipment works based on the principle of the oscillating tube [27]. To improve the accuracy of the density results, a specific calibration model is built based on the pressure, temperature, and oscillating period of the pure fluids involved in this work. The densities of each fluid (Table 2) were measured up to 30 MPa at 313.15 and 333.15 K in a dynamic flow-through mode. In addition to the individual fluids, the data of the vapor-liquid saturated densities of the systems CO<sub>2</sub>+n-butanol and CO<sub>2</sub>+n-dodecane available in previous literature [19] were also included for validation. The details of the working principle and the calibration method are explained in detail in our previous work [19]. The standard deviation of the calibration model for the CO<sub>2</sub>+n-butanol+H<sub>2</sub>O and CO<sub>2</sub>+n-dodecane+H<sub>2</sub>O ternary systems are 1.06 kg/m<sup>3</sup> and 0.908 kg/m<sup>3</sup> respectively. The combined extended density uncertainty was evaluated as a contribution of pressure, temperature, and standard deviation based on a Taylor expansion series<sup>28</sup> according to Eq. 1.

$$u_c(\rho) = \sqrt{\left(\frac{\partial \rho}{\partial P}\right)_T^2 \cdot \left(\frac{u(P)}{\rho}\right)^2 + \left(\frac{\sigma(\rho)}{\rho}\right)^2 + \left(\frac{\partial \rho}{\partial T}\right)_P^2 \cdot \left(\frac{u(T)}{\rho}\right)^2} \quad (1)$$

In this equation,  $\frac{\partial \rho}{\partial P}$  is the change of density over the change in pressure (numerically determined),  $\sigma(\rho)$  is the density standard deviation that was determined by measuring three densities for each phase, pressure, and temperature,  $u(P)$  is the pressure sensor uncertainty which was approximated to 2 %, while  $\frac{\partial \rho}{\partial T}$  is the change of density over the change in temperature and was modelled with the PCP-SAFT EoS,  $u(T)$  is the uncertainty of the temperature sensor (0.5 K). Using a coverage factor of 2, the average extended uncertainty resulting from applying Eq. 1 to the measured data resulted in 5.48 % or 11.36 kg/m<sup>3</sup>.

To assure a constant temperature inside the densimeter, the setup is positioned inside of an air heated oven. To improve heating efficiency and temperature stability, the oscillating tube unit is additionally heated by a heating re-circulator (Julabo, model CORIO CD BC4 293.15–423.15 K). The temperature is kept constant to ±0.02 K, while the pressure is kept constant at ±0.01 MPa by a syringe pump (Teledyne ISCO Syringe pump, 100DH) filled with the respective test gas.

The experiments are performed as follows: after cleaning the equipment, both liquid components (n-dodecane or n-butanol, and H<sub>2</sub>O) are pumped inside the saturation vessel. For measuring the density of the liquid phases, 20 % of the saturation vessel's volume is filled with H<sub>2</sub>O and 30 % with the organic component. For measuring the density of the vapor phase, the volume of liquid samples is reduced to half, i.e. approx. 10 and 15 % of the saturation vessel, respectively. The reduction of liquid volume decreases the chances of dragging liquid portions. Before commencing the measurement, air is purged from the system by flushing with the gas designated for the measurement three times. The temperature is set at the air heated oven and at the thermostat of the oscillating tube device. Once thermal equilibrium is achieved, the pressure is adjusted by adding the test gas using the syringe pump. No compositional analysis is performed, therefore, to assure equilibrium conditions, the phases are contacted for at least 20 hours with constant stirring at the designated pressure and temperature. In addition, temperature, pressure, and volume of the injected gas are monitored, allowing to consider thermodynamic equilibrium when these variables are constant. Before performing a measurement, the stirring unit is switched off for at least two hours to settle the system. The pressure is kept constant during equilibration as well as during the measurements.

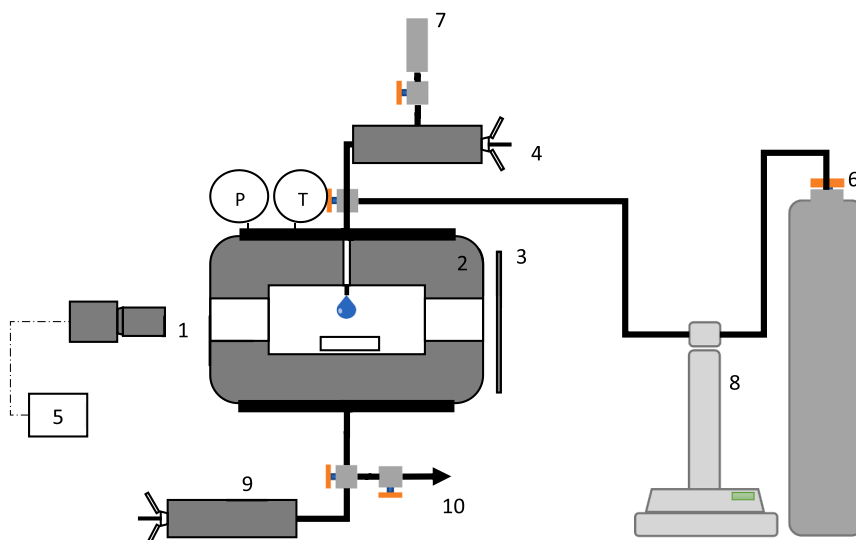


**Fig. 2.** Experimental setup for measuring interfacial tension at high pressures. The setup is comprised of a CCD (1), high– pressure view cell (2), light source (3), drop depositing unit (4), PC (5), gas cylinder (6), liquid sample container (7), automatic syringe pump (8), hand pump for heavy liquid phase (9), venting valve (10).

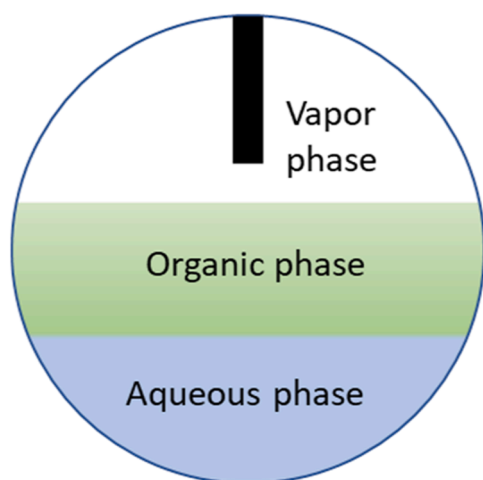


**Fig. 3.** Experimental phase layout of ternary systems. Aqueous phase (blue), organic phase (green), and vapor phase (white). For clarity, the capillary where the drop hangs is shown in black at the top of the figure.

The procedure for measuring liquid and vapor phase densities differs as for the vapor density, the test gas is injected through the bottom of the equilibration vessel at a very low flow (0.1–0.4 mL/min) in order to limit the disturbance of the phase equilibrium to a minimum, leaving the top as saturated vapor and being vented downstream of the oscillating tube device (Fig. 1). For the liquid phases, the gas is injected from the top of the saturation vessel, and it is the liquid phase that slowly flows through the densimeter to be further purged downstream. The liquid phase is passed through the oscillating tube device until the density remains at a constant value for a minimum of 30 minutes. Density, oscillation period, temperature, and pressure values are registered every 5 minutes for the vapor phase and every 2 mL purged for the liquid phases. For the coexisting liquid phases, this process is repeated until both liquid phases have passed through the oscillating tube device.

### 2.3. Interfacial tension

The interfacial tension of the aqueous-vapor and aqueous-organic interfaces of the system in this work were measured by the Pendant Drop Method [29–32], which is proved to be a suitable method to be

applied at elevated pressures and temperatures [26]. Mainly, profiles of pendant drops are optically recorded and a set of differential equations resulting from the Young-Laplace equation applied to a pendant drop [33] shown in Eq. 2 are solved by adjusting the interfacial tension in order to match the experimental drop profile.

$$\frac{1}{R_1} + \frac{1}{R_2} = \frac{2}{R} - \frac{\Delta\rho}{\gamma} \cdot g \cdot z \quad (2)$$

In Equation 2,  $g$  is the gravity acceleration,  $z$  is the length coordinate,  $\frac{1}{R_1} + \frac{1}{R_2}$  is the term representing the mean curvature of the drop,  $R$  is the curvature radii at the drop apex,  $\Delta\rho$  is the density different between the drop and surrounding phases, and  $\gamma$  is the interfacial tension.

The experiments were conducted using a high-pressure drop shape analysis system (DSA 100, Krüss GmbH) coupled with a high-pressure view cell (PDE-1700 MD-H, Eurotechnica GmbH, Germany,  $P_{\max} = 69$  MPa,  $T_{\max} = 473$  K), both depicted in Fig. 2. The high-pressure cell (2) is equipped with a pressure transducer and a thermocouple with an accuracy of  $\pm 0.01$  MPa and  $\pm 0.1^\circ\text{C}$  respectively. To allow for the drop shape observation, two windows are located at each front-end opposite to each other. A light source (1.1) is placed in front of one of the windows, while a high resolution Coupled Charged Device Camera (CCD camera, 1.2) is placed in front of the other window, opposite to the light source. The camera, thermocouple and pressure transducer are connected to a computer (4) running a drop shape analysis software (ADVANCE V.1.13; Krüss GmbH, Germany). The temperature of the view cell is regulated by an electrical heating jacket ( $T_{\max} = 473.15$  K; Hillesheim). The pressure is controlled using an automatic syringe pump (D100, Teledyne ISCO, United States, 6), connected to a high-pressure gas cylinder (7).

The methodology starts by thoroughly cleaning the view cell which is a crucial step since traces of impurities can result in strong interfacial tension deviations [34]. After the cleaning, the designated temperature is set, and the remaining air is purged using the test gas. Then, the organic component is charged first into the view cell (n-dodecane or n-butanol), followed by  $\text{H}_2\text{O}$ , both through the drop dispensing unit- $\text{H}_2\text{O}$  is injected until it forms a stable aqueous phase at the bottom of the view cell, below the vapor and organic phases, as depicted in Fig. 3. Slowly, the system is pressurized with gas until the experimental pressure is achieved. After pressure and temperature reach steady values within  $\pm 0.01$  MPa and  $\pm 0.1$  K, additional time is needed to achieve chemical equilibrium, *i.e.*, phase saturation conditions. A minimum of 1 hour is given to the  $\text{CO}_2$  containing systems to equilibrate, whereas for

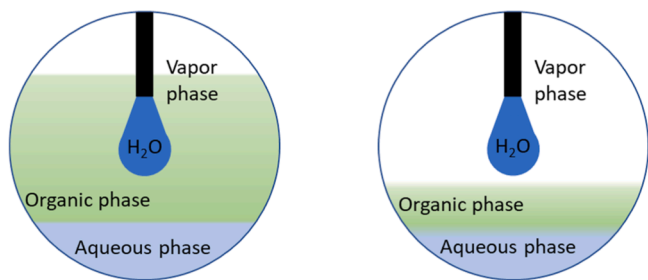


Fig. 4. Layout of the aqueous–organic (left) and vapor–aqueous (right) interfacial tension within the ternary systems.

the systems containing  $\text{CH}_4$  this time can go up to 12 hours. After the assumed equilibrium is reached, a drop is formed at the capillary with the drop dispensing unit, and recording of the drop profile is started. Once the interfacial tension is stable, three values are taken per drop at a given temperature and pressure, allowing for an uncertainty analysis to be carried out. The optical system, *i.e.*, the magnitude of the drop, is calibrated at the beginning of each measurement by optically determining the outer diameter of the capillary and relating it to the real diameter that had been determined previously by a caliper gauge.

In this work, two interfacial tensions are measured within a ternary–three component system. These interfacial tensions are the one between the organic and aqueous phase, saturated by the gas component, and between the aqueous and vapor phases, saturated by the organic component. This type of experiment is illustrated in Fig. 4. To adjust the location of the organic–vapor and organic–aqueous interfaces, the amount of organic component in the view cell is changed, and the excess of  $\text{H}_2\text{O}$  is purged through a venting valve (Fig. 2, venting valve 10). While adjusting the level of liquid phases, the pressure is kept constant by injecting the gas component with the help of the syringe pump.

Since the injection of the drop phase produces a perturbation on the equilibrated system, every drop was measured until its volume and interfacial tension were constant, *i.e.*, equilibrium was reached. This could take between 2 and 20 minutes, depending on the system. In Fig. 5 the real dynamic volumetric (as volume over initial volume) and interfacial tension data are depicted in case of two drops for the vapor–aqueous interfacial tension of the  $\text{CO}_2$ +n-butanol+ $\text{H}_2\text{O}$  system. In this case the equilibrium is reached at around 400 seconds. In this work, these dynamics are used as a confirmation of reaching equilibrium conditions in the system and are not further studied.

A minimum of five drops are measured until equilibrium, from which three consecutive values are chosen after reaching equilibrium. The interfacial tension results are corrected by multiplying the value obtained from the DSA software and the equilibrium bulk density difference of the drop and surrounding phases. The bulk densities were calculated by the PCP-SAFT for the  $\text{CO}_2$  containing systems, previously

validated by our own measurements at 313.15 and 333.15 K nearly up to the miscibility pressure between the organic and  $\text{CO}_2$  rich phases. The mixture densities of the  $\text{CH}_4$  containing systems were assumed to take the values of the respective  $\text{CH}_4$ -saturated liquid n-butanol-rich, n-dodecane-rich, and  $\text{H}_2\text{O}$ -rich phases, while the vapor phases were approximated as the  $\text{CH}_4$ -rich phase at n-butanol or n-dodecane saturation conditions from previous literature [19], neglecting the influence of water in the vapor phase. No experimental validation was performed for the ternary systems containing  $\text{CH}_4$  in this work.

The uncertainty of the interfacial tension is considered a function of the uncertainty in density experiments next to the standard deviation originating, *e.g.*, from the image quality and the quality of the mathematical fit as well as the uncertainty in temperature readings. The combined relative uncertainty,  $u_c(\gamma)$  shown in Eq. 3, is calculated based on a Taylor series expansion [28].

$$u_c(\gamma) = \sqrt{\left(\frac{1}{\gamma} \cdot \frac{\partial \gamma}{\partial P} u(p)\right)^2 + \left(\frac{u(\Delta\rho)}{\Delta\rho}\right)^2 + \left(\frac{\sigma(\gamma)}{\gamma}\right)^2 + \left(\frac{1}{\gamma} \cdot \frac{\partial \gamma}{\partial T} u(T)\right)^2} \quad (3)$$

In this equation, the derivative  $\left(\frac{\partial \gamma}{\partial P}\right)$  was determined numerically,  $u(p)$  is the standard uncertainty of pressure (0.2 %),  $u(T)$  is the uncertainty of the temperature sensor (0.5 K),  $u(\Delta\rho)$  is the density average standard uncertainty which is approximated to the one calculated from the density measurements,  $\sigma(\gamma)$  is the standard deviation of the interfacial tension. The change of interfacial tension with temperature  $\left(\frac{\partial \gamma}{\partial T}\right)$  was theoretically determined with the PCP-SAFT equation of state in combination with the DGT. The average combined relative uncertainty  $[u_c(\gamma)]$  was 1.6 % (0.29 mN/m), which results in an average expanded relative uncertainty  $[U_c(\gamma)]$  with a coverage factor of  $k=2$  and a 0.95 confidence interval of 3.3 % or 0.58 mN/m. The average standard deviation of the measurements reported in this work is 0.083 mN/m.

To further validate the accuracy of our experiments, in addition to the standard deviation and uncertainties, the Worthington number (Wo) [35,36] is calculated. This number, similar to the Bond number that additionally contains a length scale [35], compares gravitational and capillary forces on the drop.

$$\text{Wo} = \frac{(\rho_i - \rho_j) \cdot V^d \cdot g}{\pi \cdot \gamma_{ij} \cdot \varnothing_c} \quad (4)$$

The Worthington number is defined as the product of the positive phase density difference ( $\rho_i - \rho_j \geq 0$ ), the drop volume ( $V^d$ ) and the gravity acceleration constant ( $g$ ) over the product of the interfacial tension ( $\gamma_{ij}$ ) and the diameter at which the drop is attached to the capillary ( $\varnothing_c$ ). In the case of the liquid–liquid systems, the drop hung from the inner diameter of the capillary (0.5 mm), whereas for the vapor–liquid systems, the drops hung from the capillary outer diameter (1.554 mm). Even though there are no exact limit values between a good

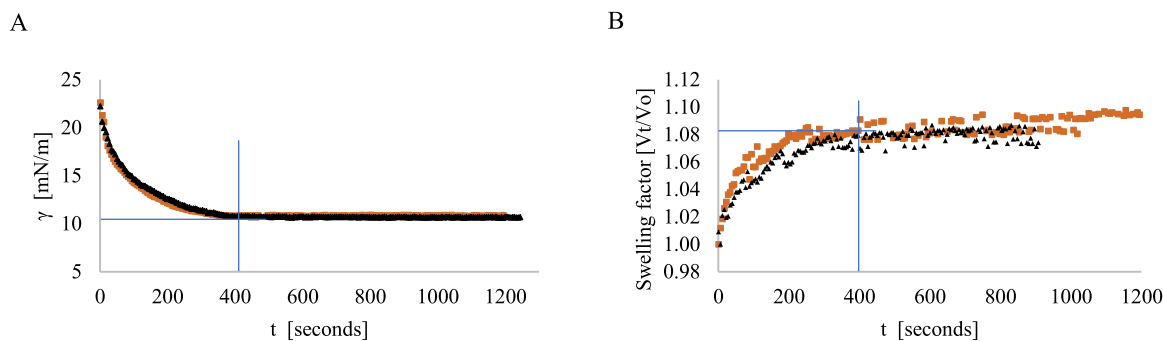


Fig. 5. Dynamic interfacial tension (A) and volumetric (B) behavior of the  $\text{H}_2\text{O}$ + $\text{CO}_2$  interface measurements on the  $\text{CO}_2$ +n-butanol+ $\text{H}_2\text{O}$  system at 313.15 K and around 7 MPa. No density correction of the interfacial tension was performed on the data depicted. The volume is shown as a ratio between the initial and dynamic one.

**Table 3**

Interfacial tension comparison of the n-butanol+H<sub>2</sub>O and n-dodecane+H<sub>2</sub>O liquid-liquid systems at atmospheric pressure.

| This work $\gamma$ mN/m          | Reference $\gamma$ mN/m | T K    |
|----------------------------------|-------------------------|--------|
| n-butanol+H <sub>2</sub> O [37]  |                         |        |
| 1.61                             | 1.59*                   | 313.15 |
| 1.08                             | 1.13**; 1.08***         | 353.15 |
| n-dodecane+H <sub>2</sub> O [33] |                         |        |
| 51.35                            | 51.24                   | 313.15 |
| 49.97                            | 50.00                   | 333.15 |
| 48.68                            | 48.5***                 | 353.15 |

\*\*at 351.33;

\*\*\*Extrapolated value

\* At 312 K;

or bad Worthington number, it is considered that values between 0.5 and 1 relate to accurate estimations of  $\gamma_{ij}$  [26,35]. The result of our experiments gives an average Wo of 0.84 [-], which means that the shape of the drops in our systems are mainly dominated by capillary forces, supporting the accuracy of our experiments.

To ensure that the method is applicable to liquid-liquid systems, the interfacial tensions between n-butanol and H<sub>2</sub>O, and between n-dodecane and H<sub>2</sub>O were measured between 313.15 and 353.15 K at atmospheric pressure and compared to previous studies (Table 3). The system n-butanol-H<sub>2</sub>O at our experimental temperatures was compared to the results of Villers & Platten [37], while the n-dodecane-H<sub>2</sub>O system was compared to the results of Zeppieri et al. [33]. Good agreement between the authors and this work is observed, deeming our pendant drop method set up as suitable to measure liquid-liquid systems.

### 3. Theoretical Framework

#### 3.1. PCP-SAFT

To estimate the phase equilibria and the respective densities of the saturated phases, the PCP-SAFT EoS based on PC-SAFT by Gross & Sadowski [38] and subsequently extended to polar compounds [39], is applied in conjunction with DGT. PCP-SAFT uses the hard-chain fluid as a reference and incorporates dispersive, polar, and associating interactions. Eq. 5 presents the Helmholtz free energy of a system as described by PCP-SAFT EoS, where  $A_{id}$  denotes the ideal contribution,  $A_{hc}$  represents the hard chain contribution,  $A_{disp}$  accounts for the dispersive force interaction contribution,  $A_{polar}$  signifies the polar contribution, and  $A_{assoc}$  includes the contribution of associating interactions.

$$A = A^{id} + A^{hc} + A^{disp} + A^{polar} + A^{assoc} \quad (5)$$

For pairs of different segments, the standard Lorentz-Berthelot [40] combining rules are used to account for the cross-dispersive interactions between the segments.

**Table 4**

Pure component PC-SAFT parameter and DGT influence parameter.

| Component                          | $M_i$ [g/mol] | $m_i$ [-] | $\sigma_i$ [Å] | $\frac{\epsilon_i}{k_B}$ [K] | $\frac{\epsilon_i^{AB}}{k_B}$ [K] | $\frac{\kappa_i^{AB}}{k_B}$ [-] | $Q_i^{i,l}$ [-] | $\kappa_{DGT}$ [ $Jm^5mol^{-2}$ ] | Reference                  |
|------------------------------------|---------------|-----------|----------------|------------------------------|-----------------------------------|---------------------------------|-----------------|-----------------------------------|----------------------------|
| CO <sub>2</sub>                    | 44.01         | 1.5131    | 3.1869         | 163.33                       | [-]                               | [-]                             | 4.4             | 2.327E-20                         | J. Gross et al. [41]       |
| H <sub>2</sub> O (4 C association) | 18.015        | 1.0656    | 3.0007         | 366.51                       | 1800                              | 0.01                            | [-]             | 0.84E-20                          | Niño-Amézquita et al. [22] |
| CH <sub>4</sub>                    | 16.043        | 1.0       | 3.7039         | 150.03                       | [-]                               | [-]                             | [-]             | 1.973E-20                         | Niño-Amézquita et al. [13] |
| n-butanol (2B association)         | 74.123        | 2.7515    | 3.6139         | 259.59                       | 2544.6                            | 0.006692                        | [-]             | 14.6E-20                          | J. Gross et al. [38]       |
| n-dodecane                         | 170.338       | 5.306     | 3.8959         | 249.21                       | [-]                               | [-]                             | [-]             | 146.563E-20                       | J. Gross et al. [40]       |
|                                    |               |           |                |                              |                                   |                                 |                 |                                   | Niño Amézquita et al. [22] |

$$[1]: Q_i^i = Q_i^2 / (m_i \epsilon_i \sigma_i^5)$$

$$\sigma_{ij} = \frac{1}{2} (\sigma_i + \sigma_j) \quad \text{Eq. 6}$$

$$\epsilon_{ij} = \sqrt{\epsilon_i \epsilon_j} \bullet (1 - k_{ij}) \quad \text{Eq. 7}$$

Thus, the segment diameter  $\sigma_{ij}$  is the arithmetic mean of the segment diameters of the individual components  $i$  and  $j$ . The depth of the pair potential  $\epsilon_{ij}$  is calculated using the geometric mean of the individual segments, with the inclusion of an additional binary interaction parameter  $k_{ij}$ . The PC-SAFT parameter can be found in Table 4.

Some considerations need to be made for the application of the parameters to the systems included in this work. The CO<sub>2</sub>+H<sub>2</sub>O system was already investigated by Nino-Amézquita et al. [13], who introduced a temperature dependent  $k_{ij}$  :

**Table 5**

Binary PC-SAFT interaction parameter and binary DGT influence parameter correction.

| Binary system                     | $k_{ij}$ | $\beta_{DGT}$ | reference                     |
|-----------------------------------|----------|---------------|-------------------------------|
| CO <sub>2</sub> +H <sub>2</sub> O | Eq. 8    | 0.25          | Niño-Amézquita et al. [13]    |
| CO <sub>2</sub> +n-butanol        | Eq. 9    | 1             | Villablanca-Ahues et al. [19] |
| CO <sub>2</sub> +n-dodecane       | 0.05     | 1             | Villablanca-Ahues et al. [19] |
| CH <sub>4</sub> +H <sub>2</sub> O | Eq. 10   | 0.55          | Niño-Amézquita et al. [20]    |
|                                   | Eq. 11   |               | Villablanca-Ahues et al. [19] |
| CH <sub>4</sub> +n-butanol        | -0.047   | 0.5           | Villablanca-Ahues et al. [19] |
| CH <sub>4</sub> +n-dodecane       | Eq. 12   | 0.3           | Niño-Amézquita et al. [13]    |
|                                   |          |               | Villablanca-Ahues et al. [19] |

**Table 6**

Binary influence parameter (DGT) of the liquid-liquid demixing.

| Binary system               | $\beta_{DGT}^{LL}$ |
|-----------------------------|--------------------|
| n-butanol+H <sub>2</sub> O  | 0.135              |
| n-dodecane+H <sub>2</sub> O | 0.135              |

**Table 7**

Results location according to properties.

| System                                       | Property                                     | Section | Tables   | Figures |
|--|--|---------|----------|---------|
| CO <sub>2</sub> +n-butanol+H <sub>2</sub> O  | $\rho$                                       | 4.2.1   | Table 5  | Fig. 8  |
|  | Phase equilibria                             | 4.1.1   | -        | Fig. 6  |
|  | $\gamma$                                     | 4.3.1   | Table 7  | Fig. 10 |
| CH <sub>4</sub> +n-butanol+H <sub>2</sub> O  | $\gamma$                                     | 4.3.2   | Table 8  | Fig. 12 |
|  | CO <sub>2</sub> +n-dodecane+H <sub>2</sub> O | $\rho$  | 4.2.2    | Table 6 |
| Phase equilibria                             |  | 4.1.2   | -        | Fig. 7  |
| $\gamma$                                     |  | 4.3.3   | Table 9  | Fig. 13 |
| CH <sub>4</sub> +n-dodecane+H <sub>2</sub> O | $\gamma$                                     | 4.3.4   | Table 10 | Fig. 14 |
|  |  |         |          | Fig. 16 |

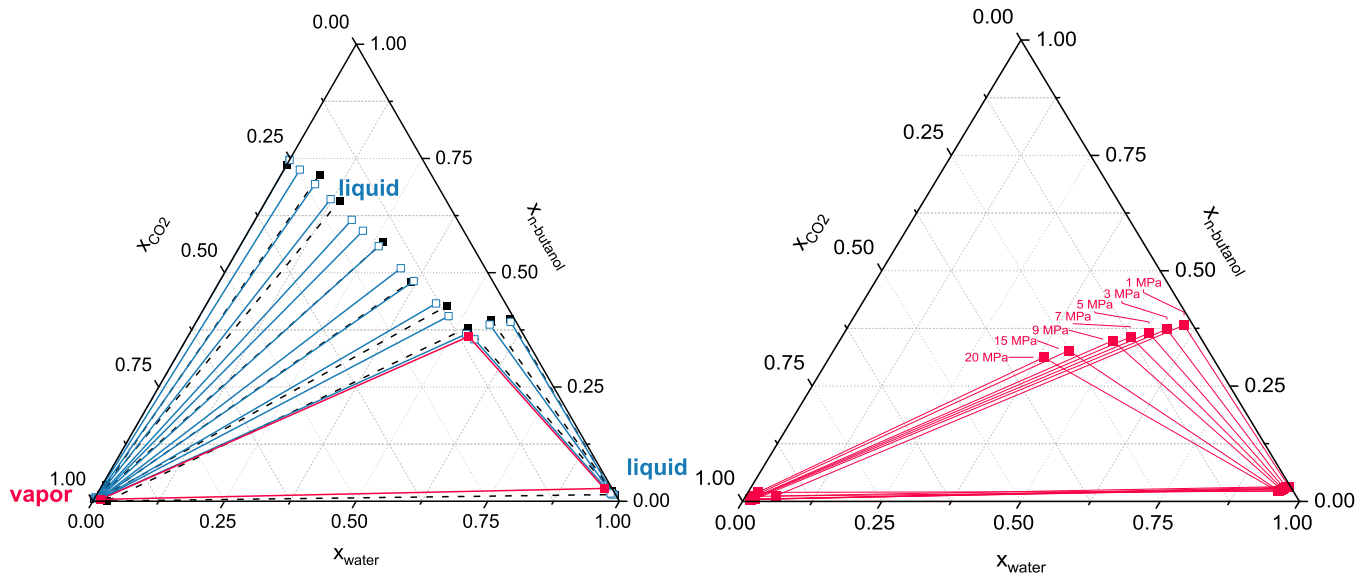


Fig. 6. VLE CO<sub>2</sub>+n-butanol-H<sub>2</sub>O: Left: The broken line with filled squares are experimental data from literature [57] at 6 MPa and 353.15 K. Blue line with open squares are two phases in equilibrium calculated using PCP-SAFT and red lines with filled squares are the three phase equilibrium calculated by PCP-SAFT. Right: Model Calculation using PCP-SAFT to quantify the size of the three-phase region in dependence of the pressure.

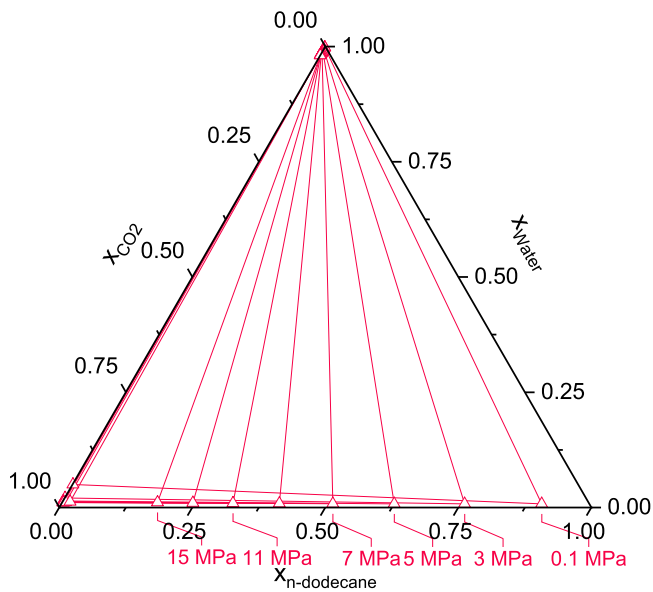


Fig. 7. Predicted VLE CO<sub>2</sub>+n-dodecane+H<sub>2</sub>O at 353.15 K: Influence of the pressure on the three-phase equilibrium calculated by PCP-SAFT.

$$k_{ij}(T) = -\frac{52.35}{T} + 0.00495 \quad (8)$$

For the CO<sub>2</sub>+n-butanol system Villablanca-Ahues et al. [19] have introduced a concentration dependent  $k_{ij}$  :

$$k_{ij} = -0.125 + 0.016 \bullet x_{CO_2} \quad (9)$$

Niño-Amezquita et al. [13] applied a concentration and temperature dependent  $k_{ij}$ , which was adapted for the CH<sub>4</sub>+H<sub>2</sub>O system:

$$k_{ij}(x_{CH_4}, T) = a_T + (0.2 - a_T)x_{CH_4} \quad (10)$$

$$a_T = -\frac{112.85}{T} + 0.228 \quad (11)$$

For the CH<sub>4</sub>+n-dodecane system also a temperature-dependent correlation of the  $k_{ij}$  was applied:

Table 8

Experimental saturated phase density of the CO<sub>2</sub>+n-butanol+H<sub>2</sub>O system.

| 313.15 K / U(p)=10.18 %     |                       |                      |                   |                            |                   |
|-----------------------------|-----------------------|----------------------|-------------------|----------------------------|-------------------|
| H <sub>2</sub> O rich phase |                       | n-butanol rich phase |                   | CO <sub>2</sub> rich phase |                   |
| P                           | $\rho$                | P                    | $\rho$            | P                          | $\rho$            |
| MPa                         | g/cm <sup>3</sup> [3] | MPa                  | g/cm <sup>3</sup> | MPa                        | g/cm <sup>3</sup> |
| 0.10                        | 0.9809                | 0.11                 | 0.8314            | 2.15                       | 0.0410            |
| 3.08                        | 0.9902                | 3.11                 | 0.8437            | 4.13                       | 0.0878            |
| 6.50                        | 0.9997                | 6.48                 | 0.8501            | 6.02                       | 0.1552            |
| 7.62                        | 1.0014                | 7.50                 | 0.8508            | 8.29                       | 0.3403            |
|                             |                       |                      |                   | 8.44                       | 0.4278            |
| 333.15 K / U(p)=2.50 %      |                       |                      |                   |                            |                   |
| H <sub>2</sub> O rich phase |                       | n-butanol rich phase |                   | CO <sub>2</sub> rich phase |                   |
| P                           | $\rho$                | P                    | $\rho$            | P                          | $\rho$            |
| MPa                         | g/cm <sup>3</sup>     | MPa                  | g/cm <sup>3</sup> | MPa                        | g/cm <sup>3</sup> |
| 0.15                        | 0.9625                | 0.15                 | 0.8164            | 2.42                       | 0.0452            |
| 3.11                        | 0.9769                | 3.12                 | 0.8232            | 4.15                       | 0.0810            |
| 6.17                        | 0.9835                | 6.12                 | 0.8278            | 6.06                       | 0.1294            |
| 9.23                        | 0.9878                | 9.24                 | 0.8287            | 8.20                       | 0.2030            |
| 11.59                       | 0.9862                | 11.61                | 0.8177            | 10.21                      | 0.3156            |
|                             |                       |                      |                   | 11.18                      | 0.4219            |

$$k_{ij}(T) = \frac{9.908}{T} - 0.012 \quad (12)$$

All other  $k_{ij}$  parameters are constant and can be found in Table 5.

### 3.2. Density gradient theory

The DGT enables the thermodynamic description of inhomogeneous systems. Hereby, the grand potential is a function of the Helmholtz energy within the inhomogeneous interfacial region. According to Cahn and Hilliard [42], the interfacial Helmholtz energy is expressed by a series expansion around the bulk phase density, making it a functional of the density gradients within the interface. In equilibrium, the grand potential is minimized. The general form of this equation for a system with N components was developed by Poser and Sanchez [43] and then adopted by Enders and Quitzsch [44]:

$$\Omega[\rho] = A[\rho] - \sum_{i=1}^N \rho_i \mu_{i,bulk} \quad (13)$$

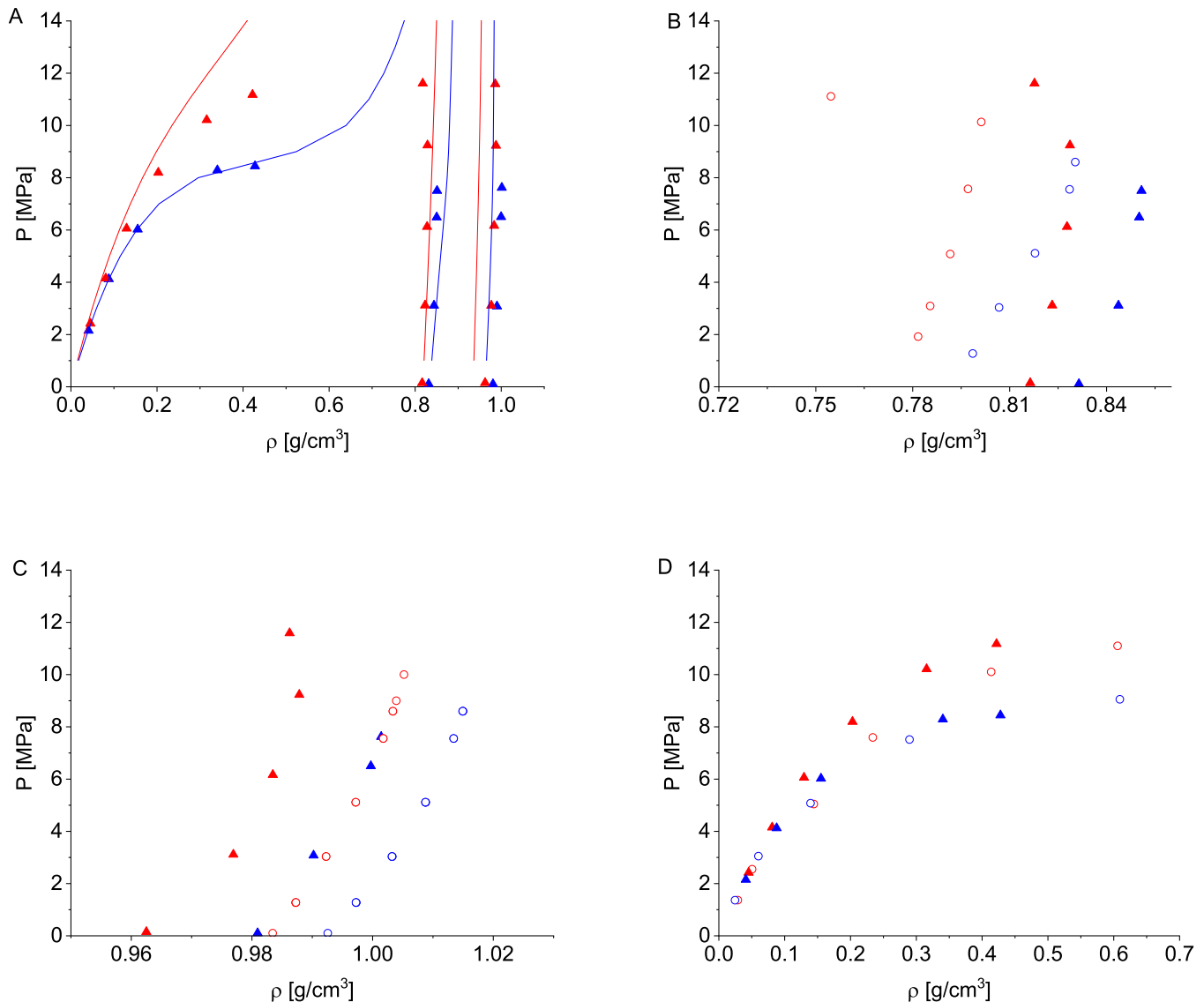


**Fig. 8.** Saturated phase density of the CO<sub>2</sub>+n-butanol+H<sub>2</sub>O system: 313.15 K (blue); 333.15 K (red); A: comparison between this work's PCP-SAFT (continuous lines) and experimental (triangles) results, B: comparison between the liquid phase of the CO<sub>2</sub>+n-butanol system (open circles) [19] and this work's n-butanol rich phase; C: comparison between the liquid phase of the CO<sub>2</sub>+H<sub>2</sub>O (open circles) [58] and this work's H<sub>2</sub>O-rich phase; D: comparison between the vapor of the CO<sub>2</sub>+n-butanol system (open circles) [19] and this work's vapor phase.

In this context  $\Omega$  denotes the grand potential,  $\mu_{i,\text{bulk}}$  represents the constant chemical potential of component  $i$ ,  $A$  refers to the molar Helmholtz energy of the inhomogeneous system, and  $\rho$  is the molar density vector formed by all the density sub-vectors of component  $i$ . Assuming a planar interface between the two phases, the equations can be simplified to a one-dimensional formulation, where only the density gradients perpendicular to the interface need to be considered. By minimizing this function using the Euler-Lagrange equations with respect to  $\rho$ , an expression for the surface tension is obtained:

$$\gamma = \int_{-\infty}^{+\infty} \Delta\Omega[\rho] \sum_{i=1}^N \sum_{j=1}^N \kappa_{ij} \frac{\partial \rho_i}{\partial z} \frac{\partial \rho_j}{\partial z} dz \quad (14)$$

Where  $\gamma$  is the surface tension,  $z$  is the direction of a planar intermediate phase in which  $\rho$  changes, and  $\kappa_{ij}$  is the influence parameter of the DGT. To calculate the interfacial tension between two corresponding phases, the integral must first be transformed from the spatial coordinate  $z$  to the density  $\rho_j$ :

$$\gamma = \int_{\rho_j^l}^{\rho_j^h} \Delta\Omega[\rho] \kappa' d\rho_j \quad (15)$$

The integration limits are converted from the complex infinity components to the bulk phase densities  $\rho_j^l$  and  $\rho_j^h$ , whereas the integration is performed numerically using a Romberg approach. For binary systems, the combined interaction parameter  $\kappa'$  can be expressed by expanding the double sum:

$$\kappa' = \kappa_j + 2\kappa_{ij} \left( \frac{d\rho_i}{d\rho_j} \right) + \kappa_i \left( \frac{d\rho_i}{d\rho_j} \right)^2 \quad (16)$$

Furthermore, an expression for the interfacial density profile over  $z$  for each density  $\rho_j^i$  between the two corresponding phases is established. Thereby, the density profile with respect to an arbitrary origin  $z_0$  is computed as:

$$z - z_0 = \int_{\rho_j^i(z_0)}^{\rho_j^i(z)} \sqrt{\frac{\kappa'}{\Delta\Omega[\rho]}} d\rho_j \quad (17)$$

**Table 9**  
Experimental saturated phase density of the CO<sub>2</sub>+n-dodecane+H<sub>2</sub>O system.

| 313.15 K / U(ρ)= 9.38 %     |                   |                       |                   |                            |                   |
|-----------------------------|-------------------|-----------------------|-------------------|----------------------------|-------------------|
| H <sub>2</sub> O rich phase |                   | n-dodecane rich phase |                   | CO <sub>2</sub> rich phase |                   |
| P                           | ρ                 | P                     | ρ                 | P                          | ρ                 |
| MPa                         | g/cm <sup>3</sup> | MPa                   | g/cm <sup>3</sup> | MPa                        | g/cm <sup>3</sup> |
| 0.05                        | –                 | 0.11                  | 0.7381            | 1.02                       | 0.0151            |
| 2.08                        | 0.9974            | 2.19                  | 0.7458            | 3.13                       | 0.0581            |
| 5.23                        | 1.0038            | 5.22                  | 0.7609            | 6.29                       | 0.1595            |
| 7.15                        | 1.0065            | 7.21                  | 0.7727            | 7.55                       | 0.2625            |
| 9.05                        | 1.0075            | 9.25                  | 0.7865            | 8.21                       | 0.3587            |
| 333.15 K / U(ρ)=3.13 %      |                   |                       |                   |                            |                   |
| H <sub>2</sub> O rich phase |                   | n-dodecane rich phase |                   | CO <sub>2</sub> rich phase |                   |
| P                           | ρ                 | P                     | ρ                 | P                          | ρ                 |
| MPa                         | g/cm <sup>3</sup> | MPa                   | g/cm <sup>3</sup> | MPa                        | g/cm <sup>3</sup> |
| 0.13                        | 0.9817            | 0.14                  | 0.7276            | 0.74                       | 0.0149            |
| 0.14                        | 0.9816            | 3.39                  | 0.7306            | 2.16                       | 0.0397            |
| 0.14                        | 0.9817            | 6.06                  | 0.7353            | 5.11                       | 0.1018            |
| 3.21                        | 0.9864            | 9.62                  | 0.7449            | 7.98                       | 0.1926            |
| 6.12                        | 0.9900            | 12.17                 | 0.7367            | 10.17                      | 0.3137            |
| 9.60                        | 0.9933            |                       |                   | 12.19                      | 0.5085            |

The binary influence factor  $\kappa_{ij}$  is calculated via a modified geometric mixing rule:

$$\kappa_{ij} = \beta \sqrt{\kappa_i \kappa_j} \quad (18)$$

Here,  $\beta$  is an additional parameter adjusted to one experimental data point of the interfacial tension. In the case that  $\beta$  is equal to 1, the mixing rule reduces to the simple geometric mixing rule and the interfacial tension can be predicted. Mixtures including H<sub>2</sub>O often require non-unity values for  $\beta$  to model the interfacial tension in good accordance with the interfacial tension reported by Niño-Amezquita and Enders [13, 20]. In the case of liquid-liquid interface a  $\kappa_{DGT}^{LL}$  is applied, which can be calculated as follows:

$$\kappa_{DGT}^{LL} = \beta_{DGT}^{LL} \sum_{i=1}^N \sum_{j=1}^N \kappa_{ij} \frac{\partial \rho_i}{\partial z} \frac{\partial \rho_j}{\partial z} \quad (19)$$

Hereby the  $\beta_{DGT}^{LL}$  is adjusted to the experimental data point of the binary demixing system as shown in Table 6:

For a more detailed derivation of the DGT, the interested reader can take a look at R. Evans [45] or at the work of Poser and Sanchez [43]. For liquid-liquid (incompressible) systems, the following works could be interesting [44,46,47]. Several implementations of the DGT have been applied in literature, combining it with various EoS [13,20,22,48–52] or g<sup>E</sup>-models [53–56]. To accommodate the systems investigated within the scope of this study, the DGT is coupled to the PCP-SAFT EoS.

## 4. Results and Discussion

In the following section, the experimental and theoretical results on phase equilibria, saturated bulk densities and interfacial tension, starting by showing the phase equilibria results, predicted by the PCP-SAFT EoS (4.1). The density results are shown next, in Section 4.1, while the interfacial tensions are presented in Section 4.3. A summary of the sections, tables and figures containing our results are shown in Table 7. It is worth mentioning that the interfacial tension measurement, as well as the density measurement were performed at vapor-liquid-liquid equilibrium.

### 4.1. Phase Equilibria

This section presents the modeling of phase equilibrium with PCP-SAFT. The experimental data are relatively sparse in the literature. Data is only available for the CO<sub>2</sub>+n-butanol+H<sub>2</sub>O system. For this reason, this system is used for the validation of PCP-SAFT, and the remaining phase equilibria are predicted, whereas we have taken the

PCP-SAFT parameter as well as the influence parameter for the DGT from our previous work [19].

#### 4.1.1. CO<sub>2</sub>+n-butanol+ H<sub>2</sub>O

Fig. 6 (left) shows the phase equilibrium of CO<sub>2</sub>+n-butanol-water with the experimental measurement data of Chen et al. [58] and the comparison with the predictions of PCP-SAFT at 6 MPa and 353.15 K. Here it becomes clear that PCP-SAFT can reproduce the phase behaviour in the two-phase region as well as in the three-phase region with high accuracy starting from the binary subsystems. Since this system is the most complex of the systems due to the polarity of CO<sub>2</sub> and the hydrogen bonding of water and n-butanol, we assume that all other systems can principally be predicted in a similarly good way, relying on the PCP-SAFT EoS. In Fig. 6 (right), a model calculation using PCP-SAFT is presented, showing the influence of an increasing pressure on the ternary phase behaviour. As expected, the three-phase region shrinks as the pressure rises, but the tie line in the LLE gets longer. This also indicates higher interfacial tension.

#### 4.1.2. CO<sub>2</sub>+n-dodecane+H<sub>2</sub>O

Fig. 7 shows the three-phase region of CO<sub>2</sub>+n-dodecane-water at 353.15 K as a function of different pressures. Here, too, the three-phase region becomes smaller at higher pressures and the solubility of CO<sub>2</sub> is increased accordingly.

## 4.2. Saturated phase density

In this section, the measured densities in the three-phase regions, i.e., at vapor-liquid-liquid equilibrium, are presented and compared to the PCP-SAFT modeling. The strategy used here is similar to that for determining the phase equilibria: If the model can predict the densities of the systems containing CO<sub>2</sub> well, it is assumed that the systems with CH<sub>4</sub> will also principally work with similar deviations from experimental data Table 8.

#### 4.2.1. CO<sub>2</sub>+n-butanol+ H<sub>2</sub>O

The results of the saturated phase density of the ternary system comprising CO<sub>2</sub>, n-butanol, and H<sub>2</sub>O are depicted in Fig. 8 and Table 9. In Fig. 8 A, the overall phase density results from our experiments are shown along with the model results. Fig. 8 B includes the saturated organic density of the CO<sub>2</sub>+n-butanol, while Fig. 8 C includes the modelled determined aqueous density of the H<sub>2</sub>O+CO<sub>2</sub> system [58]. Lastly, Fig. 8 D shows the comparison between the vapor phases of the ternary system and the CO<sub>2</sub>+n-butanol vapor phase density. In Fig. 8 A the saturated phase density results from the PCP-SAFT (continuous line) are compared to the experimental results (triangles). Both approaches agree quite well in temperature and pressure trends, especially for the 313.15 K isotherm. There is an underprediction of the theoretical calculations for the aqueous phase density, while at the same time an overprediction of the organic phase's density occurs. Disagreements between the theoretical and experimental approaches are found at the vapor phase at 333.15 K, over 8 MPa. These disagreements result in different locations of the apparent miscibility pressure between predictions and experiments. The origin of this disagreement is the simultaneous prediction of the vapor-liquid and vapor-liquid-liquid equilibria. It is well known that the prediction of the vapor phase density is in better agreement compared to the density of the liquid phases [15].

The vapor density of the CO<sub>2</sub>+n-butanol+H<sub>2</sub>O system increases as pressure increases, i.e., when the organic and vapor phases approach total miscibility. An increasing temperature results in a decrease in the vapor phase density. When comparing the vapor phase of the ternary three component system with the vapor phase of the binary two component CO<sub>2</sub>+n-butanol system, a slight decrease in the ternary system's vapor density is observed. Nevertheless, this change is quite modest, not showing a strong influence of H<sub>2</sub>O on the saturated vapor density compared to the CO<sub>2</sub>+n-butanol system. By comparing the

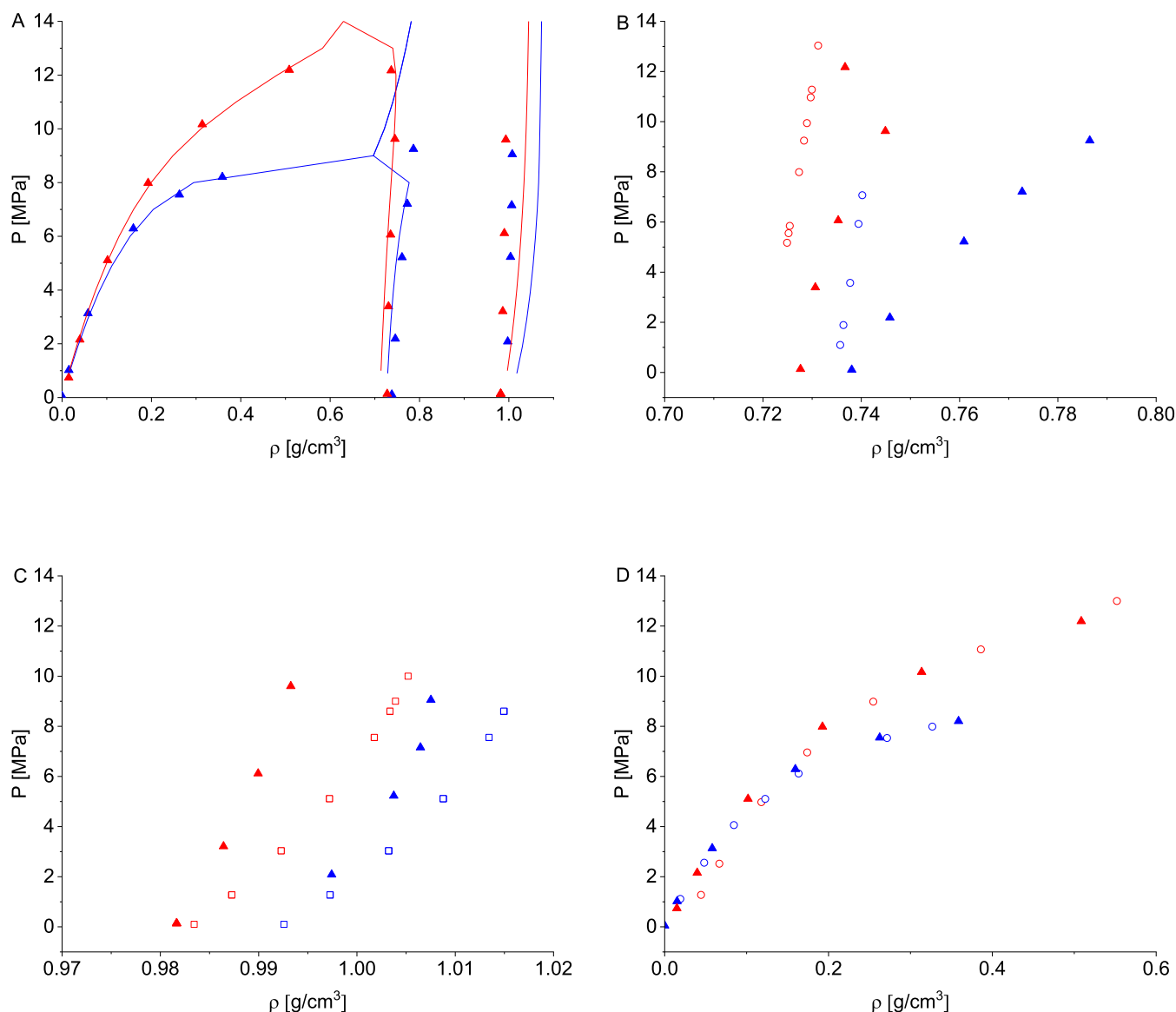


**Fig. 9.** Saturated phase density of the  $\text{CO}_2$ +n-dodecane+ $\text{H}_2\text{O}$  system: 313.15 K (blue); 333.15 K (red); A: comparison between PCP-SAFT (continuous lines) and this work's experimental results (triangles), B: comparison between the liquid phase of the  $\text{CO}_2$ +n-dodecane system (open circles) [19] and this work's n-dodecane rich phase; C: comparison between the liquid phase of the  $\text{CO}_2$ + $\text{H}_2\text{O}$  (open circles) [58] and this work's  $\text{H}_2\text{O}$ -rich phase; D: comparison between the vapor of the  $\text{CO}_2$ +n-dodecane system (open circles) [19] and this work's vapor phase.

organic and aqueous phases of the ternary systems to the organic and aqueous phases of the  $\text{CO}_2$ +n-butanol and  $\text{CO}_2$ + $\text{H}_2\text{O}$  systems respectively, the effect of  $\text{H}_2\text{O}$  in the organic phase (Fig. 8 C) and the effect of n-butanol in the aqueous phase of the ternary system (Fig. 8 B) can be assessed. Based on the fact that pressure has only little influence on liquid systems, the effect of  $\text{CO}_2$  over the liquid densities can be related to the pressure-density trends in the liquid densities. The organic density of the ternary system increases as pressure increases, while the opposite trend is observed with temperature. The aqueous density of the ternary system increases with increasing pressure, parallel to the density-pressure increase of the  $\text{H}_2\text{O}$ + $\text{CO}_2$  system's liquid phase. A shift to smaller densities of the aqueous phase of the ternary system compared to the aqueous phase of the two-component system  $\text{H}_2\text{O}$ + $\text{CO}_2$  is observed due to the n-butanol content. The same effect is observed in the organic phase, where a parallel density-pressure increase between the organic phase of the  $\text{CO}_2$ +n-butanol system and the organic phase of the ternary system is found. Contrary to the aqueous phase of the ternary system, its organic phase is shifted to higher densities compared to the aqueous

phase of the  $\text{CO}_2$ +n-butanol system, showing that the content of  $\text{H}_2\text{O}$  increases its density. The trends are observed in both isotherms and for the entire range of pressure studied. The parallel pressure-density trend suggests that the mutual solubility of  $\text{H}_2\text{O}$  and n-butanol is not enhanced by the  $\text{CO}_2$  content in the mixture, that on its turn is directly related to the pressure. A similar trend can be seen from the phase behavior calculation in Fig. 6 (right). So, the PCP-SAFT results show that the tie line of LLE in the three phase regions gets longer with increasing pressure. Both results indicate that the solubility of n-butanol in water is reduced by the increase in pressure and the increased concentration of  $\text{CO}_2$ . This behavior will be further discussed when referring to the interfacial tension of the  $\text{CO}_2$ +n-butanol+ $\text{H}_2\text{O}$  system.

#### 4.2.2. $\text{CO}_2$ +n-dodecane+ $\text{H}_2\text{O}$

The results of the saturated phase density of the ternary system comprising  $\text{CO}_2$ , n-dodecane, and  $\text{H}_2\text{O}$  are depicted in Fig. 9 and Table 9. In Fig. 9 A experimental and model results are compared to each other. Fig. 9 B shows a comparison of the binary  $\text{CO}_2$ +n-dodecane and the

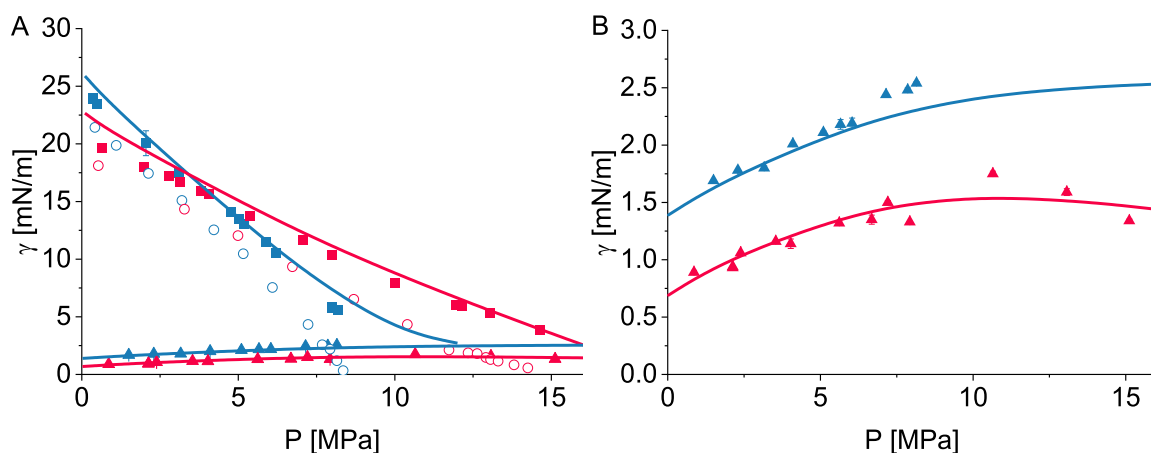


**Fig. 10.** Aqueous-organic and vapor-aqueous interfacial tension of the system  $\text{CO}_2$ +n-butanol+ $\text{H}_2\text{O}$  at 313.15 K (blue) and 353.15 K (red). A: This work vapor-aqueous interface (squares); this work organic-aqueous interface (triangles);  $\text{CO}_2$ +n-butanol interfacial tension [19] (open circles). B: scaled interfacial tension of the aqueous-organic interface.

**Table 10**

Interfacial tension of the  $\text{H}_2\text{O}$ -n-butanol and  $\text{H}_2\text{O}$ - $\text{CO}_2$  interfaces in the  $\text{CO}_2$ +n-butanol+ $\text{H}_2\text{O}$  system.

| $\text{CO}_2$ +n-butanol+ $\text{H}_2\text{O}$ / 313.15 K            |          |               |  |          |               |
|--|----------|---------------|--|----------|---------------|
| $\text{H}_2\text{O}$ - $\text{CO}_2$ interface / $U(\gamma)= 3.33\%$ |          |               | $\text{H}_2\text{O}$ -n-butanol interface / $U(\gamma)= 13.48\%$ |          |               |
| P  | $\gamma$ | std. $\gamma$ | P  | $\gamma$ | std. $\gamma$ |
| MPa  | mN/m     | mN/m          | MPa  | mN/m     | mN/m          |
| 0.35   | 24.00    | 9.97E-02      | 1.50   | 1.69     | 6.71E-04      |
| 0.35   | 23.94    | 1.08E-01      | 2.30   | 1.78     | 7.08E-04      |
| 0.47   | 23.47    | 2.25E-01      | 3.16   | 1.80     | 1.84E-02      |
| 2.05   | 20.06    | 1.08          | 4.10   | 2.01     | 2.16E-03      |
| 3.09   | 17.48    | 4.19E-01      | 5.10   | 2.11     | 1.33E-02      |
| 4.78   | 14.07    | 9.25E-03      | 5.66   | 2.18     | 4.20E-02      |
| 5.01   | 13.51    | 1.50E-01      | 6.04   | 2.19     | 4.55E-02      |
| 5.18   | 13.02    | 1.53E-02      | 7.15   | 2.44     | 6.60E-04      |
| 5.88   | 11.46    | 1.28E-01      | 7.86   | 2.48     | 1.81E-02      |
| 6.19   | 10.50    | 1.28E-02      | 8.15   | 2.54     | 1.28E-02      |
| 7.98   | 5.81     | 1.76E-02      |  |          |               |
| 7.99   | 5.80     | 6.26E-03      |  |          |               |
| 8.00   | 5.77     | 3.05E-03      |  |          |               |
| 8.00   | 5.78     | 6.37E-03      |  |          |               |
| 8.18   | 5.62     | 1.03E-02      |  |          |               |
| $\text{CO}_2$ +n-butanol+ $\text{H}_2\text{O}$ / 353.15 K            |          |               |  |          |               |
| $\text{H}_2\text{O}$ - $\text{CO}_2$ interface / $U(\gamma)= 2.50\%$ |          |               | $\text{H}_2\text{O}$ -n-butanol interface / $U(\gamma)= 14.15\%$ |          |               |
| P  | $\gamma$ | std. $\gamma$ | P  | $\gamma$ | std. $\gamma$ |
| MPa  | mN/m     | mN/m          | MPa  | mN/m     | mN/m          |
| 0.64   | 19.61    | 2.36E-02      | 0.86   | 0.89     | 1.71E-02      |
| 2.00   | 17.96    | 9.68E-02      | 2.13   | 0.94     | 2.65E-03      |
| 2.77   | 17.22    | 9.41E-03      | 2.13   | 0.93     | 5.02E-03      |
| 3.15   | 16.66    | 9.22E-03      | 2.39   | 1.06     | 1.99E-03      |
| 3.80   | 15.94    | 8.42E-02      | 2.39   | 1.06     | 6.61E-04      |
| 4.06   | 15.62    | 6.15E-02      | 3.54   | 1.16     | 3.02E-03      |
| 5.37   | 13.76    | 1.66E-02      | 4.03   | 1.14     | 4.14E-02      |
| 7.06   | 11.70    | 7.34E-02      | 5.62   | 1.32     | 1.81E-02      |
| 7.98   | 10.37    | 5.48E-02      | 6.68   | 1.35     | 3.98E-02      |
| 10.00  | 7.92     | 6.75E-03      | 7.21   | 1.50     | 1.51E-02      |
| 11.96  | 6.06     | 8.19E-04      | 7.93   | 1.33     | 6.19E-04      |
| 12.16  | 5.95     | 4.35E-02      | 10.65  | 1.75     | 2.27E-02      |
| 13.03  | 5.33     | 1.52E-02      | 13.07  | 1.59     | 2.96E-02      |
| 14.63  | 3.88     | 7.83E-02      | 15.12  | 1.34     | 1.43E-02      |

ternary  $\text{CO}_2$ +n-dodecane+ $\text{H}_2\text{O}$  systems, while Fig. 9 C compares the aqueous phase of the ternary and the two component  $\text{H}_2\text{O}$ + $\text{CO}_2$  system. Lastly, Fig. 9 D depicts the vapor phase of the ternary system and the  $\text{CO}_2$ +n-dodecane vapor density.

The model and experimental results satisfactorily agree, even though the aqueous density is overpredicted by the model, while the organic phase is slightly underpredicted. In general, the density increases with decreasing temperature and with increasing pressure, a trend that

inverts for the organic phase in the proximities of the miscibility pressure, where increasing pressure decreases the organic phase's density. Contrary to the theoretical results of the  $\text{CO}_2$ +n-butanol+ $\text{H}_2\text{O}$  system, the PCP-SAFT EoS appears to underpredict the solubility between n-dodecane and  $\text{H}_2\text{O}$ . The location of the miscibility pressures according to experiments and theory agree better in this system than in the  $\text{CO}_2$ +n-butanol+ $\text{H}_2\text{O}$  system.

With respect to pressure, the vapor density of the ternary system has a similar trend compared to the ternary system containing n-butanol, *i.e.*, a higher density as pressure increases, a trend that is enhanced as the organic-vapor phases miscibility pressure is approached. No influence on the vapor density is observed in the ternary system due to the  $\text{H}_2\text{O}$  content when comparing to the  $\text{CO}_2$ +n-dodecane system's vapor phase. The organic phase of the ternary system's density increases with increasing pressure. Comparing the organic phase of the ternary system with the organic phase of the two component  $\text{CO}_2$ +n-dodecane system, the density of the binary-organic and the ternary-organic phase start from a common value close to 0.1 MPa. As pressure increases, the phase densities diverge, *i.e.*, the density increase of the ternary-organic phase is faster than the binary-organic phase. For the aqueous phase of the ternary system, its density also increases with increasing pressure, although compared to the aqueous phase of the  $\text{H}_2\text{O}$ + $\text{CO}_2$  system, the influence of the pressure on the density is less. The stronger influence of the pressure on the density of the organic phase compared to the aqueous phase suggests that the solubility between  $\text{H}_2\text{O}$  and n-dodecane is enhanced as the concentration of  $\text{CO}_2$  increases in both liquid phases.

#### 4.3. Interfacial tension

In this chapter, the modeling and experimental results for the interfacial tension at vapor-liquid-liquid equilibrium conditions are reviewed. Here, the calculated interfacial tensions for the vapor-liquid systems are predicted using the density gradient theory combined to the PCP-SAFT EoS.

##### 4.3.1. $\text{CO}_2$ +n-butanol+ $\text{H}_2\text{O}$

The interfacial tension of the ternary system comprising  $\text{CO}_2$ , n-butanol, and  $\text{H}_2\text{O}$ , specifically its vapor-aqueous and organic-aqueous interfaces, are depicted in Fig. 10 and Table 10. In Fig. 10 A both interfacial tensions are shown. In addition, the results of the interfacial tension of the  $\text{CO}_2$ +n-butanol are included. Given the low interfacial tension of the organic-aqueous interface, these values are zoomed in Fig. 10 B.

In this work, the vapor-aqueous interfacial tension of the ternary system exhibits a decreasing trend as pressure increases for both

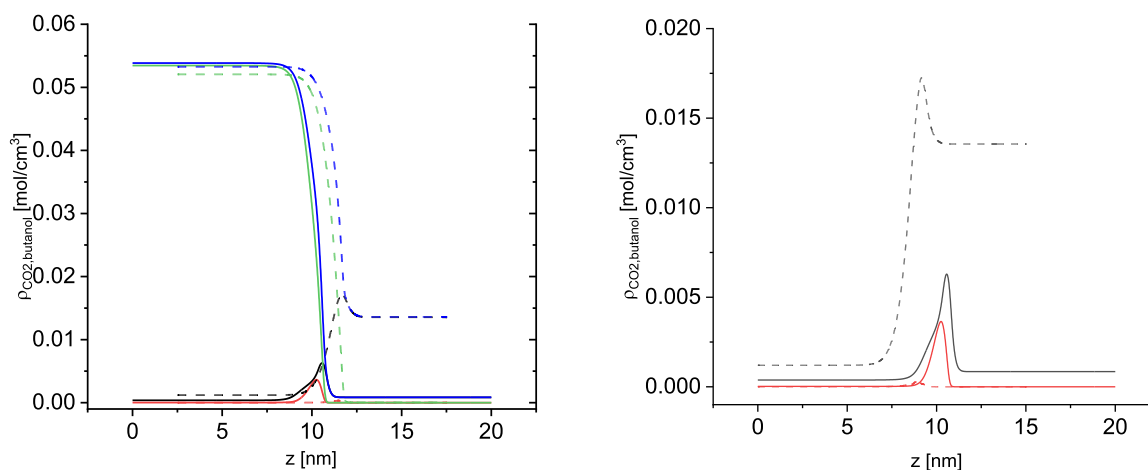


Fig. 11. Comparison of interfacial density profiles between vapor and aqueous phase in the CO<sub>2</sub>+n-butanol+H<sub>2</sub>O ternary system at 2 MPa (continuous lines) and 10 MPa (dashed lines) at 313.15 K. Left: CO<sub>2</sub> (black line), n-butanol (red line), H<sub>2</sub>O (green line) density profiles as well as the total mixture density (blue line); Right: magnification with only CO<sub>2</sub> and butanol enrichment shown.

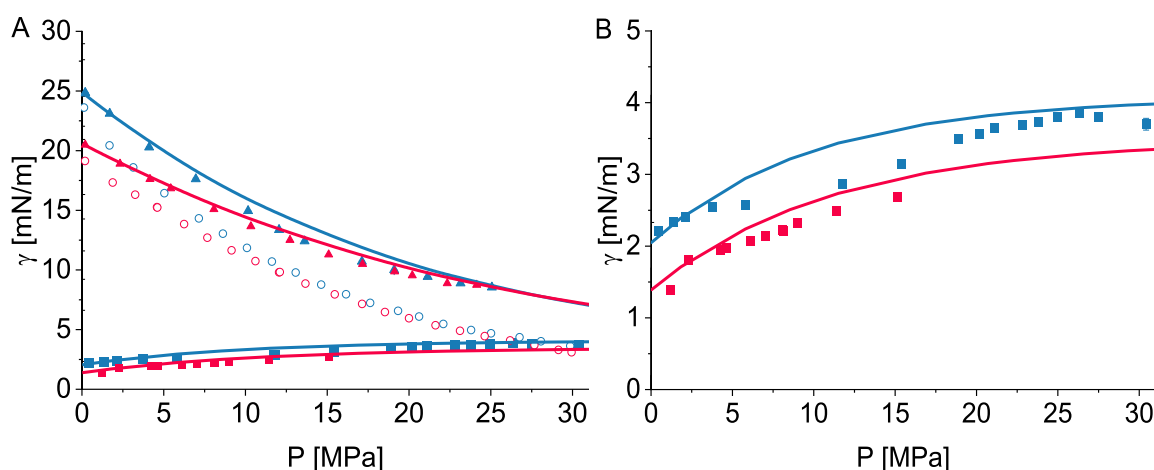


Fig. 12. Aqueous-organic and vapor-aqueous interfacial tension of the system CH<sub>4</sub>+n-butanol+H<sub>2</sub>O at 313.15 (blue) and 353.15 K (red). A: aqueous-organic interface (squares), aqueous-vapor interface (triangles), CH<sub>4</sub>+n-butanol [19] (open circles), modelled results (PCP-SAFT+DGT; continuous lines). B: zoomed organic-aqueous interfacial tension.

isotherms. A temperature-interfacial tension crossover is observed at around 3 MPa. Below this pressure, at lower temperature the interfacial tension increases, while this trend is inverted at pressures above 3 MPa. The interfacial tension of the ternary's vapor-aqueous interface behaves almost identical to that of the CO<sub>2</sub>+n-butanol system at the same pressures and temperatures instead of resembling the H<sub>2</sub>O+CO<sub>2</sub> interfacial tension [31].

The decreasing organic – aqueous interfacial tension with increasing temperature can be explained by the increased solubility of 1-butanol in the aqueous phase [57]. While the increasing interfacial tension at elevated pressures is related to the longer tie lines in the phase equilibrium (Fig. 7) of the liquid–liquid system. The interfacial tension of the VLE and LLE is also modelled using the PCP-SAFT EoS in the DGT framework. It becomes obvious, that the trend in the interfacial tension of the VLE is predicted in a high quality, but there are some deviations from the experiments especially at low pressures at 353.15 K. One reason could be that there are higher deviations in the density. Furthermore, the interfacial tension of the LLE is quantitatively predicted with the maximum in the interfacial tension.

To further explain the observations made at the vapor-aqueous interface, the density profile of CO<sub>2</sub>, H<sub>2</sub>O, and n-butanol through this interface are calculated with the PCP-SAFT+DGT approach and shown

in Fig. 11 at two pressures, 2 MPa and 10 MPa at 313.15 K.

It is evident that the enrichment of n-butanol at the interface significantly decreases from 2 MPa to 10 MPa. In addition, the location of the n-butanol enrichment is between the aqueous side of the interface and the peak of CO<sub>2</sub>. These adjacent peaks of n-butanol and CO<sub>2</sub> explain the interfacial tension taking values in the order of the binary CO<sub>2</sub>+n-butanol interfacial tension. While the absolute value of the CO<sub>2</sub> density increases within the interface due to the higher CO<sub>2</sub> bulk phase density at 10 MPa, the enrichment of CO<sub>2</sub> at the interface with respect to the bulk phase densities decreases significantly. This supports the previous conclusions based on measured vapor-aqueous interfacial tension in the presence of n-butanol (Fig. 10), which is dominated by the binary CO<sub>2</sub>+butanol interfacial tension. Even at higher pressures near 10 MPa, where n-butanol exhibits almost no enrichment, CO<sub>2</sub>-enrichment is significantly reduced compared to the binary CO<sub>2</sub>+H<sub>2</sub>O systems [13], thereby retaining similarly low interfacial tension that still seem to be governed by CO<sub>2</sub>+n-butanol interactions within the interface, rather than by the H<sub>2</sub>O-CO<sub>2</sub> interface. Furthermore, competitive enrichment is assumed to take influence on dynamic properties, such as diffusivities and interfacial mass transfer properties, which will be investigated in a subsequent study.

**Table 11**

Interfacial tension of the H<sub>2</sub>O–n-butanol and H<sub>2</sub>O–CH<sub>4</sub> interfaces in the H<sub>2</sub>O+n-butanol+CH<sub>4</sub> system.

| CH <sub>4</sub> +n-butanol+H <sub>2</sub> O / 313.15 K |      |          |   |       |          |
|--|------|----------|---|-------|----------|
| H <sub>2</sub> O–n-butanol interface / U(γ)= 6.02 %    |      |          | H <sub>2</sub> O–CH <sub>4</sub> interface / U(γ)= 1.13 % |       |          |
| P  | γ    | std.γ    | P   | γ     | std.γ    |
| MPa  | mN/m | mN/m     | MPa   | mN/m  | mN/m     |
| 0.45   | 2.21 | 2.24E-03 | 0.20  | 24.85 | 4.49E-02 |
| 1.35   | 2.33 | 2.09E-03 | 0.20  | 24.81 | 5.90E-02 |
| 2.12   | 2.41 | 1.18E-03 | 1.70  | 23.11 | 2.94E-02 |
| 3.75   | 2.54 | 1.32E-03 | 4.11  | 20.28 | 1.99E-02 |
| 5.81   | 2.57 | 1.22E-03 | 6.96  | 17.62 | 6.69E-02 |
| 11.77  | 2.86 | 1.52E-03 | 10.16   | 14.95 | 1.56E-02 |
| 11.78  | 2.87 | 1.49E-03 | 12.05   | 13.36 | 1.81E-02 |
| 15.39  | 3.14 | 5.47E-03 | 13.62   | 12.41 | 2.17E-02 |
| 18.88  | 3.49 | 1.70E-03 | 17.12   | 10.71 | 5.12E-02 |
| 20.19  | 3.57 | 1.74E-03 | 19.09   | 10.00 | 4.51E-03 |
| 21.08  | 3.64 | 1.82E-03 | 21.14   | 9.43  | 1.42E-02 |
| 22.82  | 3.69 | 1.72E-03 | 23.15   | 8.89  | 1.21E-02 |
| 23.78  | 3.73 | 4.41E-03 | 25.07   | 8.54  | 5.90E-02 |
| 24.96  | 3.80 | 3.34E-03 |   |       |          |
| 26.36  | 3.86 | 1.82E-03 |   |       |          |
| 27.49  | 3.80 | 1.30E-02 |   |       |          |
| 30.42  | 3.70 | 8.19E-02 |   |       |          |
| CH <sub>4</sub> +n-butanol+H <sub>2</sub> O / 353.15 K |      |          |   |       |          |
| H <sub>2</sub> O–n-butanol interface / U(γ)= 6.90 %    |      |          | H <sub>2</sub> O–CH <sub>4</sub> interface / U(γ)= 2.00 % |       |          |
| P  | γ    | std.γ    | P   | γ     | std.γ    |
| MPa  | mN/m | mN/m     | MPa   | mN/m  | mN/m     |
| 1.22   | 1.39 | 5.64E-02 | 0.20  | 20.49 | 2.27E-01 |
| 2.28   | 1.80 | 1.28E-02 | 2.33  | 18.90 | 1.42E-02 |
| 4.24   | 1.94 | 3.88E-03 | 4.16  | 17.61 | 7.00E-02 |
| 4.65   | 1.98 | 2.63E-03 | 5.43  | 16.83 | 9.49E-03 |
| 6.14   | 2.07 | 5.45E-03 | 8.07  | 15.09 | 1.90E-02 |
| 7.04   | 2.14 | 4.96E-03 | 10.33   | 13.65 | 1.34E-02 |
| 8.10   | 2.23 | 1.85E-02 | 12.72   | 12.51 | 5.14E-03 |
| 8.14   | 2.21 | 3.21E-02 | 15.09   | 11.29 | 2.56E-02 |
| 8.98   | 2.32 | 6.24E-03 | 17.16   | 10.50 | 4.89E-03 |
| 11.42  | 2.49 | 1.38E-03 | 19.12   | 9.87  | 6.01E-02 |
| 15.13  | 2.69 | 1.53E-03 | 20.20   | 9.54  | 1.24E-02 |
|  |      |          | 22.34   | 8.88  | 5.27E-02 |
|  |      |          | 24.14   | 8.75  | 4.56E-03 |

#### 4.3.2. CH<sub>4</sub>+n-butanol+H<sub>2</sub>O

The interfacial tension of the aqueous-organic and vapor-aqueous interfaces of the system comprising CH<sub>4</sub>, n-butanol, and H<sub>2</sub>O are depicted in Fig. 12 and Tables 11 and 12. In Fig. 12 A, the interfacial tension of the two interfaces studied in this work are shown as a function of pressure comparing the results of this work to the two component CH<sub>4</sub>+n-butanol system at the same temperature. In Fig. 12 B the results are zoomed for better reading.

This system exhibits a converging interfacial tension-pressure trend between the organic–aqueous and the aqueous–vapor interfaces up to 15 MPa, beyond which a weak pressure-dependent interfacial tension is observed. At enhanced temperature the interfacial tension is decreased for both interfaces, having little influence for pressures above 10 MPa. Even though CH<sub>4</sub> is hardly soluble in the liquid phases compared to CO<sub>2</sub>, the organic–aqueous interfacial tension increases as pressure rises, in analogy to what is found for the aqueous-organic interfacial tension in the CO<sub>2</sub>+n-butanol+H<sub>2</sub>O system. The increasing concentration of CH<sub>4</sub> in the liquid bulk phases results in a competitive adsorption between n-butanol and CH<sub>4</sub> at the aqueous interface, especially as pressure increases, as observed in the CO<sub>2</sub>+n-butanol+H<sub>2</sub>O system. Nevertheless, this effect is quite modest, being n-butanol that dominates the adsorption directly at the aqueous side of the interface.

The aqueous-vapor interface of this system, instead of exhibiting an “CH<sub>4</sub>+H<sub>2</sub>O” interfacial tension value, shows values resembling the “CH<sub>4</sub>+n-butanol” system, proving again the preferential adsorption of n-butanol at the aqueous side of the interface. The aforementioned behavior changes at around 10 MPa, where the “CH<sub>4</sub>+n-butanol”-like interfacial tension shown by the ternary system departs towards higher

**Table 12**

Interfacial tension of the H<sub>2</sub>O–n-dodecane and H<sub>2</sub>O–CO<sub>2</sub> interfaces in the H<sub>2</sub>O+n-dodecane+CO<sub>2</sub> system.

| CO <sub>2</sub> +n-dodecane+H <sub>2</sub> O / 313.15 K |       |          |   |       |          |
|---|-------|----------|---|-------|----------|
| H <sub>2</sub> O–n-dodecane interface / U(γ)= 6.46 %    |       |          | H <sub>2</sub> O–CO <sub>2</sub> interface / U(γ)= 2.37 % |       |          |
| P   | γ     | std.γ    | P   | γ     | std.γ    |
| MPa   | mN/m  | mN/m     | MPa   | mN/m  | mN/m     |
| 0.10  | 51.35 | 2.00E-02 | 0.65  | 66.18 | 4.24E-01 |
| 0.66  | 45.65 | 2.54E-02 | 1.65  | 59.97 | 4.27E-02 |
| 1.33  | 42.60 | 7.99E-02 | 2.21  | 54.55 | 5.22E-02 |
| 2.17  | 40.23 | 1.28E-01 | 3.27  | 50.49 | 9.38E-02 |
| 4.13  | 34.14 | 3.44E-02 | 3.71  | 48.56 | 1.14E-01 |
| 5.97  | 31.38 | 7.79E-02 | 4.19  | 46.06 | 4.35E-02 |
| 7.90  | 27.86 | 1.49E-01 | 4.77  | 44.18 | 9.70E-02 |
|   |       |          | 5.32  | 42.07 | 8.31E-02 |
|   |       |          | 6.38  | 38.26 | 6.84E-02 |
|   |       |          | 7.31  | 34.57 | 1.43E-01 |
|   |       |          | 8.09  | 31.98 | 1.21E-02 |
| CO <sub>2</sub> +n-dodecane+H <sub>2</sub> O / 353.15 K |       |          |   |       |          |
| H <sub>2</sub> O–n-dodecane interface / U(γ)= 6.23 %    |       |          | H <sub>2</sub> O–CO <sub>2</sub> interface / U(γ)= 2.67 % |       |          |
| P   | γ     | std.γ    | P   | γ     | std.γ    |
| MPa   | mN/m  | mN/m     | MPa   | mN/m  | mN/m     |
| 0.10  | 48.68 | 2.00E-02 | 0.52  | 59.76 | 2.17E-02 |
| 5.13  | 33.31 | 4.20E-02 | 0.62  | 59.42 | 1.25E-01 |
| 7.32  | 32.13 | 3.56E-02 | 1.16  | 57.86 | 3.15E-02 |
| 0.83  | 42.75 | 6.49E-01 | 1.67  | 56.82 | 6.78E-02 |
| 2.22  | 40.09 | 1.93E-01 | 2.06  | 55.91 | 3.60E-01 |
| 3.83  | 36.46 | 1.48E-01 | 2.44  | 55.11 | 1.00E-01 |
| 6.09  | 32.99 | 5.57E-02 | 3.17  | 53.17 | 1.26E-01 |
| 8.12  | 31.35 | 9.53E-03 | 4.12  | 49.98 | 1.14E+00 |
| 10.14   | 28.68 | 9.78E-02 | 5.31  | 46.88 | 8.52E-01 |
| 12.18   | 26.96 | 6.95E-02 | 5.77  | 45.75 | 1.62E-01 |
| 12.18   | 26.94 | 1.27E-01 | 6.31  | 44.35 | 4.83E-01 |
|   |       |          | 7.23  | 42.07 | 4.29E-01 |
|   |       |          | 8.24  | 40.04 | 4.69E-01 |
|   |       |          | 10.38   | 35.52 | 3.37E-01 |
|   |       |          | 12.16   | 32.43 | 3.67E-02 |
|   |       |          | 13.08   | 31.71 | 2.37E-03 |
|   |       |          | 14.08   | 29.69 | 2.77E-02 |

values. In analogy to the CO<sub>2</sub>+n-butanol+H<sub>2</sub>O system, this behavior is explained by a decrease in the n-butanol adsorption at the interface as the vapor and organic phases increase their miscibility. The prediction of the interfacial tension of the VLE applying PCP-SAFT in combination with the DGT is in good accordance with the experimental data, being able to predict the interfacial tension crossover. At a first glance also the interfacial tension of the LLE could be predicted in good accordance with the experimental data, even if there are some deviations regarding the shoulder in the interfacial tension Fig. 12 B.

#### 4.3.3. CO<sub>2</sub>+n-dodecane+H<sub>2</sub>O

The experimental values of the interfacial tension as well those predicted by the PCP-SAFT+DGT approach of the aqueous-vapor interface of the system comprising CO<sub>2</sub>, n-dodecane, and H<sub>2</sub>O are depicted in Fig. 13 and Table 9. The experimental organic-aqueous interfacial tension data of the same system are further included. As a further comparison, the interfacial tension data on the respective binary subsystems are also shown.

Both interfaces studied in this ternary system exhibit a decreasing interfacial tension at elevated pressures, leveling out at higher pressures. In the case of the aqueous-vapor interfacial tension, the data can be predicted with high accuracy using PCP-SAFT, but there are some deviations for the interfacial tension of the LLE. The experimental and predicted aqueous-vapor interfacial tension of the CO<sub>2</sub>+n-dodecane+H<sub>2</sub>O system behaves similar to the predicted CO<sub>2</sub>+H<sub>2</sub>O interfacial tension, contrary to what was observed in the aqueous-vapor interface of the CO<sub>2</sub>+n-butanol+H<sub>2</sub>O system. This can be explained by the fact that no liquid phase rich in CO<sub>2</sub> is formed, and CO<sub>2</sub> does not accumulate as strongly at the interface. However, the ternary aqueous-vapor interfacial

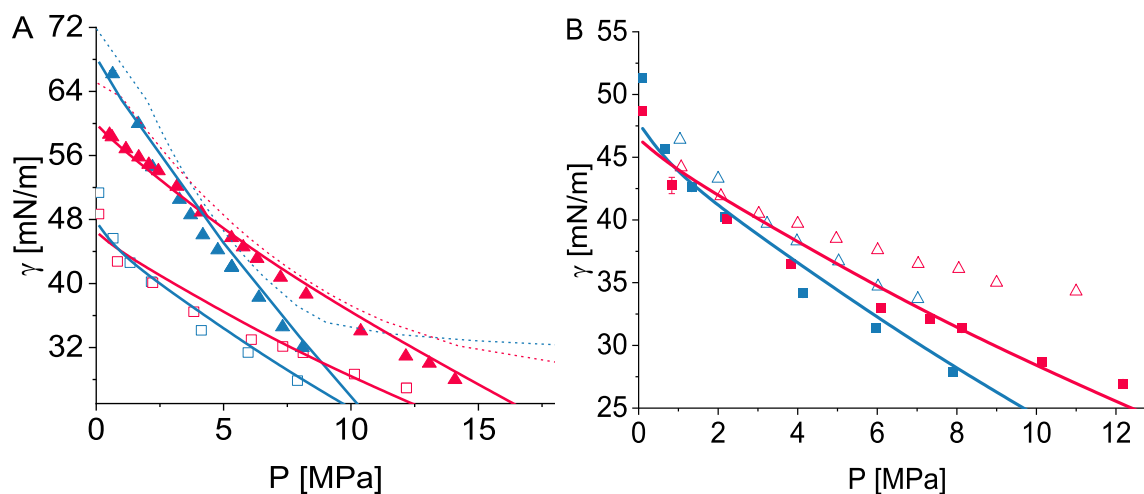


**Fig. 13.** Aqueous-organic, organic-vapor, and vapor-aqueous interfacial tension of the  $\text{CO}_2$ +n-dodecane+ $\text{H}_2\text{O}$  system at 313.15 K (blue) and 353.15 K (red). A: vapor-aqueous interface (triangles) and organic-aqueous interface (open squares); theoretical interfacial tension of the  $\text{CO}_2$ + $\text{H}_2\text{O}$  system based on the parameters of Villablanca-Ahues et al. [19] (dotted line); This work's theoretical results (PCP-SAFT+DGT predictions; continuous lines). B: zoomed aqueous-organic interfacial tension; Pan & Trusler [59]: organic-aqueous interfacial tension of the  $\text{CO}_2$ +n-decane+ $\text{H}_2\text{O}$  system (open triangles) at 313.15 K (blue) and 353.15 K (red), and organic-aqueous interface results in this work (open squares), PCP-SAFT+DGT predictions (continuous lines).

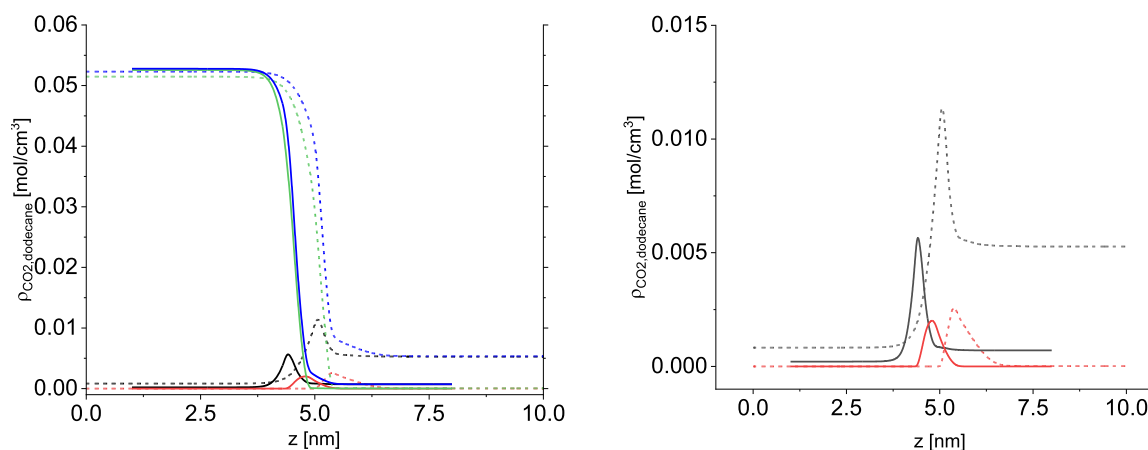


**Fig. 14.** Comparison of interfacial density profiles between vapor and aqueous interface in the  $\text{CO}_2$ +n-dodecane+ $\text{H}_2\text{O}$  ternary system at 2 MPa (continuous line) and 10 MPa (dashed line) at 313.15 K. Left:  $\text{CO}_2$  (black lines), n-dodecane (red lines),  $\text{H}_2\text{O}$  (green lines) and the total mixture (blue lines) interfacial densities; Right: scaled version with only  $\text{CO}_2$  and n-dodecane enrichment.

tension shows a small offset of around 4 mN/m with respect to the  $\text{CO}_2$ + $\text{H}_2\text{O}$  system. The interfacial tension between the liquid phases also decreases continuously with increasing pressure. This can be related to the phase behavior, as the tie lines become shorter with increasing pressure due to the solubilizing  $\text{CO}_2$  (Fig. 7). The interfacial tensions of both interfaces appear to converge as the miscibility of the organic-vapor phase is approached, in analogy to the mixture densities. In the case of the vapor-aqueous interface, there is a temperature-crossover at around 3 MPa, up to which a lower temperature results in higher interfacial tensions. Beyond the crossover, higher temperatures result in higher interfacial tension, analogous to the vapor-aqueous interfacial tension of the  $\text{CO}_2$ +n-butanol+ $\text{H}_2\text{O}$  system.

The interfacial tension of the organic-aqueous interface shows a decrease at elevated pressures, while at pressures below 2 MPa, higher temperatures result in lower interfacial tensions, a trend that is inverted beyond 2 MPa. The apparent temperature crossover found in the aqueous-organic interface of the  $\text{CO}_2$ +n-dodecane+ $\text{H}_2\text{O}$  system has been previously described for a similar system by Pan & Trusler [59]. They measured the organic-aqueous interfacial tension of the ternary system comprising  $\text{CO}_2$ , n-decane, and  $\text{H}_2\text{O}$ , finding a temperature

crossover of the same characteristics at roughly the same pressure (Fig. 13 B). They explain this crossover from the perspective of the bulk phases, by considering that the solubility of  $\text{CO}_2$  in the liquid phases increases at lower temperatures, resulting in an enhanced influence of pressure on the solubility of  $\text{CO}_2$ , lowering the interfacial tension. In addition, the decreasing interfacial tension at elevated pressures may be explained by considering the observations of Choudhary et al. [60], who found that  $\text{CO}_2$  adsorbs preferentially at the interface of n-decane. Transferring their findings to this system,  $\text{CO}_2$  may be interpreted as acting like an organic-aqueous surfactant, decreasing the hydrophobic-hydrophilic repulsion between n-dodecane and  $\text{H}_2\text{O}$ .

To further support and explain the observations made at the vapor-aqueous interface, the density profiles of  $\text{CO}_2$ ,  $\text{H}_2\text{O}$ , and n-dodecane across the interface are theoretically calculated with the PCP-SAFT+DGT approach at 2 MPa and 10 MPa at 313.15 K are shown in Fig. 14.

In contrast to the system with n-butanol, the small n-dodecane enrichment does not decrease with increasing pressure and it is located on the vapor ( $\text{CO}_2$ -rich) side of the interface. Moreover,  $\text{CO}_2$  enrichment with respect to the bulk phase is significantly higher in the n-dodecane

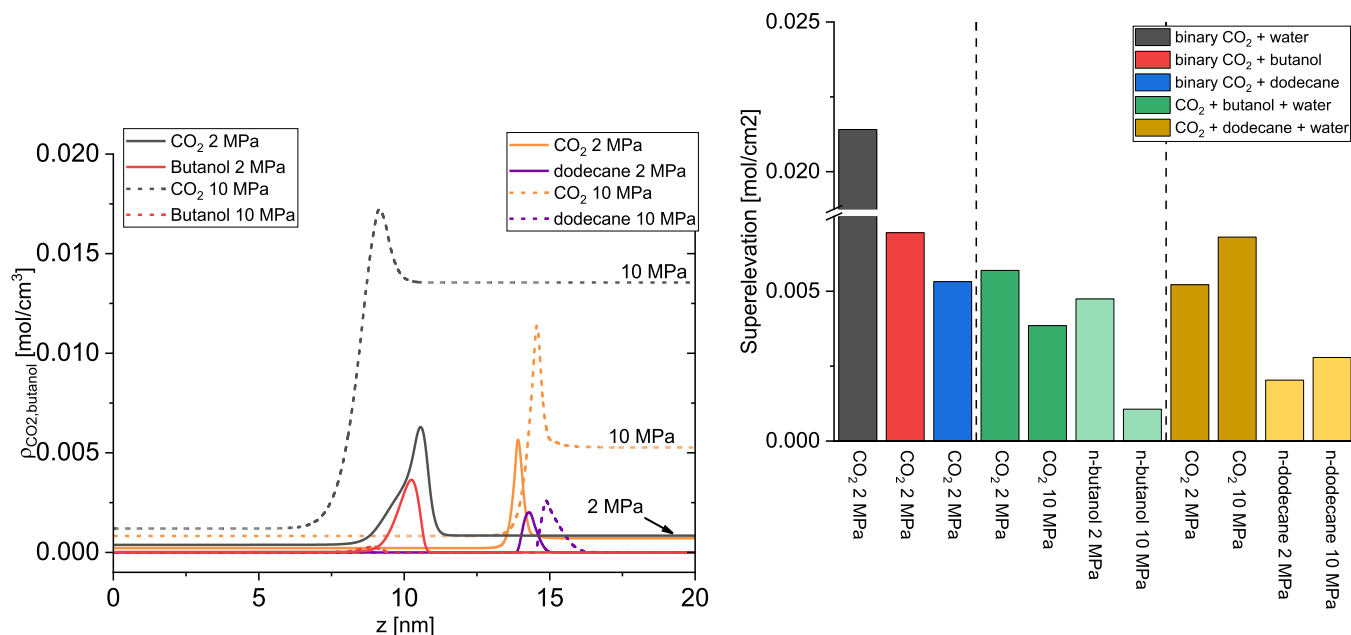


Fig. 15. Left: Comparison of CO<sub>2</sub>, n-butanol and n-dodecane enrichment in the CO<sub>2</sub>+butanol+H<sub>2</sub>O (black and red lines) and CO<sub>2</sub>+n-dodecane+H<sub>2</sub>O (orange and purple lines) at 2 MPa (continuous lines) and 10 MPa (dashed lines) at 313.15 K. Right: interfacial enrichment with respect to the bulk phase based on Eq. 20.

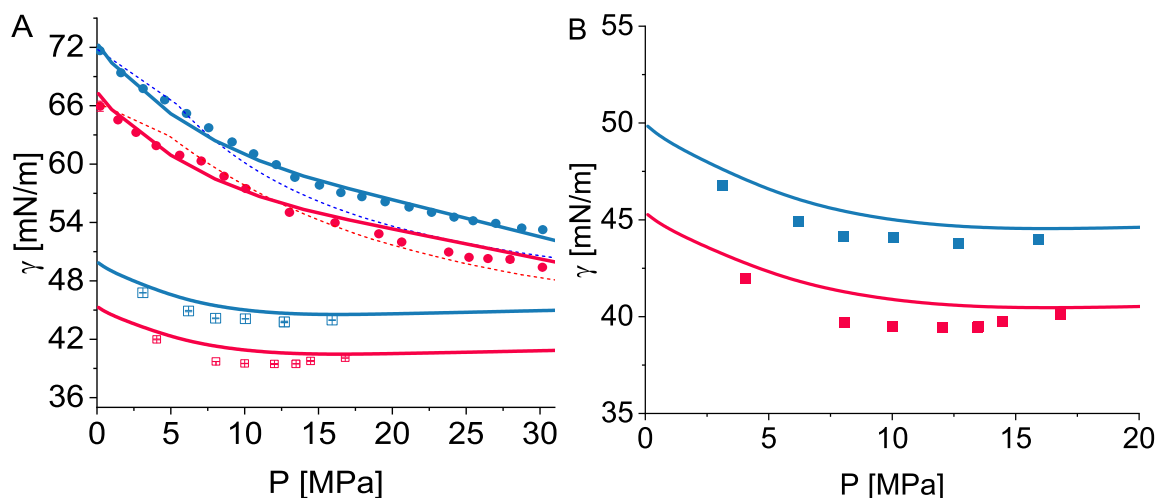


Fig. 16. Aqueous-organic and vapor-aqueous interfacial tension of the system CH<sub>4</sub>+n-dodecane+H<sub>2</sub>O at 313.15 (blue) and 353.15 K (red). A: experimental aqueous-organic interface (squares) and aqueous-vapor interface (circles), PCP-SAFT+DGT results of the CH<sub>4</sub>+H<sub>2</sub>O [19] system (dotted lines), PCP-SAFT+DGT results for the aqueous-vapor interfacial tension of the CH<sub>4</sub>+n-dodecane+H<sub>2</sub>O (continuous lines). B: zoomed organic-aqueous interfacial tension.

system compared to when paired with n-butanol (Fig. 11), suggesting CO<sub>2</sub> and n-dodecane to mutually enhance their enrichment. This finding explains why the aqueous-vapor interfacial tension tends to resemble a CO<sub>2</sub>+H<sub>2</sub>O rather than CO<sub>2</sub>+n-dodecane interfacial tension. For clarity, a comparison of CO<sub>2</sub>, butanol and dodecane enrichment in their respective ternary systems with H<sub>2</sub>O is depicted in Fig. 15. The enrichment with respect to the bulk phase densities in Fig. 15 is expressed as a “superelevation” which is consistent to our previous investigations of enrichment behavior in liquid-liquid systems [46,47,61]. Thereby, the superelevation  $SE$  of component  $i$  is defined in this work as the difference between the maximum enrichment and the maximum bulk phase density as outlined in Eq. 20.

$$SE_i = \rho_{i,max} - \max(\rho_i^I, \rho_i^{II}) \quad (20)$$

Observing the different behavior in the two systems with respect to the enrichment of the organic and gas components it becomes evident

that n-dodecane – while also enriching at the vapor-aqueous interface – does not exhibit displacing properties against CO<sub>2</sub>, resulting in a co-adsorption rather than a competitive adsorption. The co-adsorption of n-dodecane at the aqueous-vapor interface is further supported by the lowered interfacial tension by around 4 mN/m in relation to the CO<sub>2</sub>+H<sub>2</sub>O system [19].

#### 4.3.4. CH<sub>4</sub>+n-dodecane+H<sub>2</sub>O

The results on interfacial tension of the system comprising CH<sub>4</sub>, n-dodecane, and H<sub>2</sub>O are depicted in Fig. 16 and Table 13.

The vapor-aqueous interface of the CH<sub>4</sub>+n-butanol+H<sub>2</sub>O system shows a decreasing interfacial tension as pressure and temperature increase. Compared to the same system containing CO<sub>2</sub> instead of CH<sub>4</sub>, the effect of pressure and temperature are modest. PCP-SAFT in combination with the DGT can predict the interfacial tension of the VLE and LLE in good accordance with the experimental data. Also, the minimum in

**Table 13**

Interfacial tension of the H<sub>2</sub>O–n-dodecane and H<sub>2</sub>O–CH<sub>4</sub> interfaces in the H<sub>2</sub>O+n-dodecane+CH<sub>4</sub> system.

| CH <sub>4</sub> +n-dodecane+H <sub>2</sub> O / 313.15 K |       |          |   |       |          |
|---|-------|----------|---|-------|----------|
| H <sub>2</sub> O–n-dodecane interface / U(γ)= 5.16 %    |       |          | H <sub>2</sub> O–CH <sub>4</sub> interface / U(γ)= 1.78 % |       |          |
| P   | γ     | std.γ    | P   | γ     | std.γ    |
| MPa   | mN/m  | mN/m     | MPa   | mN/m  | mN/m     |
| 3.11  | 46.78 | 1.26E-02 | 1.64  | 66.32 | 2.83E-02 |
| 6.21  | 44.90 | 7.12E-02 | 1.03  | 68.06 | 1.84E-02 |
| 8.04  | 44.16 | 3.71E-02 | 2.14  | 65.58 | 4.60E-02 |
| 10.05   | 44.10 | 1.15E-02 | 2.70  | 64.91 | 6.62E-03 |
| 12.69   | 43.76 | 2.69E-02 | 3.14  | 64.08 | 2.14E-01 |
| 12.69   | 43.78 | 7.50E-02 | 3.63  | 63.33 | 3.14E-02 |
| 15.93   | 43.96 | 2.75E-02 | 4.29  | 62.83 | 2.48E-02 |
|   |       |          | 4.65  | 62.20 | 3.46E-02 |
|   |       |          | 5.15  | 61.73 | 8.68E-03 |
|   |       |          | 5.62  | 61.43 | 1.23E-01 |
|   |       |          | 6.15  | 60.85 | 7.83E-02 |
|   |       |          | 7.14  | 60.12 | 4.19E-02 |
|   |       |          | 8.22  | 59.03 | 5.59E-02 |
|   |       |          | 9.18  | 58.45 | 6.35E-02 |
|   |       |          | 10.25   | 57.36 | 1.48E-01 |
|   |       |          | 12.18   | 56.35 | 8.04E-02 |
|   |       |          | 12.72   | 55.76 | 1.06E-02 |
|   |       |          | 13.66   | 55.30 | 1.35E-01 |
|   |       |          | 15.20   | 54.38 | 5.20E-02 |
|   |       |          | 16.23   | 53.78 | 3.67E-02 |
|   |       |          | 17.75   | 53.17 | 2.76E-02 |
|   |       |          | 19.21   | 52.47 | 4.45E-02 |
|   |       |          | 21.13   | 51.78 | 4.21E-03 |
|   |       |          | 22.75   | 51.00 | 1.72E-02 |
|   |       |          | 24.16   | 50.34 | 2.43E-02 |
|   |       |          | 25.24   | 50.15 | 2.34E-02 |
|   |       |          | 25.69   | 49.97 | 1.31E-02 |

| CH <sub>4</sub> +n-dodecane+H <sub>2</sub> O / 353.15 K |       |          |   |       |          |
|---|-------|----------|---|-------|----------|
| H <sub>2</sub> O–n-dodecane interface / U(γ)= 5.48 %    |       |          | H <sub>2</sub> O–CH <sub>4</sub> interface / U(γ)= 1.81 % |       |          |
| P   | γ     | std.γ    | P   | γ     | std.γ    |
| MPa   | mN/m  | mN/m     | MPa   | mN/m  | mN/m     |
| 4.04  | 41.98 | 1.72E-01 | 0.32  | 60.88 | 3.99E-02 |
| 8.06  | 39.71 | 4.08E-02 | 2.21  | 58.71 | 2.48E-01 |
| 10.00   | 39.51 | 3.40E-03 | 6.77  | 54.28 | 3.74E-01 |
| 12.02   | 39.46 | 1.99E-02 | 4.13  | 56.61 | 6.06E-03 |
| 16.82   | 40.10 | 4.75E-02 | 10.18   | 51.83 | 1.28E-01 |
| 14.47   | 39.77 | 5.72E-02 | 10.18   | 51.83 | 2.91E-02 |
| 13.48   | 39.48 | 4.25E-02 | 14.37   | 49.25 | 1.47E-01 |
| 13.47   | 39.46 | 1.54E-02 | 16.20   | 48.40 | 8.23E-02 |
|   |       |          | 18.14   | 47.48 | 6.49E-02 |
|   |       |          | 18.14   | 47.46 | 1.98E-01 |
|   |       |          | 20.72   | 46.15 | 3.40E-01 |
|   |       |          | 22.61   | 45.64 | 9.33E-02 |
|   |       |          | 24.69   | 45.30 | 6.91E-02 |

the interfacial tension of the LLE can be predicted. The vapor-aqueous interface of the ternary system behaves very much alike the binary system H<sub>2</sub>O+CH<sub>4</sub>. This means that n-dodecane does not enrich at the aqueous side of the interface, not competing nor co-adsorbing with CH<sub>4</sub>. The effect of n-dodecane over the CH<sub>4</sub>+H<sub>2</sub>O interfacial tension is smaller than the effect of n-dodecane over the CO<sub>2</sub>+H<sub>2</sub>O interfacial tension.

The aqueous–organic interfacial tension decreases as pressure does, *i.e.*, CH<sub>4</sub> concentration, although not as strong as in the case of CO<sub>2</sub>. It appears that at pressures beyond 7 MPa there is no influence of pressure on the organic-aqueous interfacial tension. This was previously observed by Kodera *et al.* [6] in the system containing CH<sub>4</sub>, H<sub>2</sub>O, and n-decane starting at 2 MPa and 283.2 and 298.2 K. The interfacial tension value to which the organic-aqueous interface seems to converge amounts to 45 mN/m at 313.15 K and 40 mN/m at 333.15 K. In general, CH<sub>4</sub> weakly adsorbs at the interface between n-dodecane and H<sub>2</sub>O, with no effect beyond 7 MPa, as also the concentration of CH<sub>4</sub> is generally low in the aqueous phase [19,62].

## 5. Conclusions

The interfacial behavior of systems containing self-, cross-, and non-associating fluids was investigated at enhanced gas pressures in the context of subsurface energy systems. The phase equilibria of the ternary systems comprising CO<sub>2</sub> were successfully predicted by the PCP-SAFT EoS based on binary interactions parameters. The mixture densities and interfacial tensions show good agreement between measured and calculated values, unless arriving close to the pressure of complete miscibility. The experimental phase densities suggest that the influence of CO<sub>2</sub> on the solubility between H<sub>2</sub>O and n-butanol is negligible, while it does enhance the solubility between n-dodecane and H<sub>2</sub>O.

The aqueous-vapor interfacial tensions of the ternary systems containing n-butanol resemble that of the (CO<sub>2</sub> or CH<sub>4</sub>)+n-butanol systems. As pressure increases, the ternary system's vapor-aqueous interfacial tension deviates from the respective n-butanol+gas system to higher values. The n-butanol+H<sub>2</sub>O interfacial tension increases at elevated pressures, *i.e.*, as the CH<sub>4</sub> or CO<sub>2</sub> concentration increases in the liquid phases. The aqueous-vapor interfacial tension of the ternary systems containing n-dodecane resembles, for CH<sub>4</sub> and CO<sub>2</sub>, the behavior of the H<sub>2</sub>O+gas systems. As pressure increases, the vapor-aqueous interfacial tension of the ternary systems decreases, not deviating much from their corresponding H<sub>2</sub>O+gas system. The n-dodecane+H<sub>2</sub>O interfacial tension decreases at elevated pressure, showing some surfactant capabilities of CH<sub>4</sub> and CO<sub>2</sub> at this interface.

The experimental observations and the PCP-SAFT+DGT calculation of the vapor-aqueous interfacial density profile indicate a co-adsorbs of n-dodecane and CO<sub>2</sub> at the aqueous interface, while it is observed a competitive adsorption between n-butanol and the gas components.

The interfacial composition and the resulting interfacial properties are assumed to have a strong impact on the mass transport across fluid interfaces, for which the dynamic behavior in terms of dynamic interfacial tension, drop swelling and mass transport coefficients is subject to the current investigation to be reported soon.

### CRedit authorship contribution statement

**R. Villablanca-Ahues:** Validation, Formal analysis, Methodology, Data curation, Writing – original draft, Visualization. **R. Nagl:** Visualization, Investigation. **T. Zeiner:** Writing – review & editing, Supervision, Funding acquisition. **P. Jaeger:** Writing – review & editing, Supervision, Project administration, Funding acquisition.

### Declaration of Competing Interest

The authors declare the following financial interests/personal relationships which may be considered as potential competing interests: Philip Jaeger reports financial support was provided by German Research Foundation. Tim Zeiner reports financial support was provided by Austrian Science Fund. If there are other authors, they declare that they have no known competing financial interests or personal relationships that could have appeared to influence the work reported in this paper.

### Data Availability

Data will be made available on request.

### Acknowledgement

This work was financed by the DFG (Deutsche Forschungsgemeinschaft), grant number JA 871/2-1, and the FWF (Fond zur Förderung der wissenschaftlichen Forschung), project number I 5347, as part of the joint project Interfaces and Mass Transfer at Elevated Pressure.

## List of symbols

|                |                                    |  |
|----------------|------------------------------------|--|
| Symbol         | Unit                               | Description  |
| AJ             | mol                                | Free energy  |
| $k_{ij}$       |                                    | binary interaction parameter for dispersive forces         |
| Mg             | mol <sup>-1</sup>                  | molar mass   |
| RJ             | K <sup>-1</sup> mol <sup>-1</sup>  | universal gas constant                                     |
| TK             |                                    | absolute temperature                                       |
| xmol           | mol <sup>-1</sup>                  | molar fraction   |
| zm             |                                    | interfacial coordinate                                     |
| PMPa           |                                    | Pressure   |
| $u_c$          |                                    | Combined relative uncertainty                              |
| $U_c$          |                                    | Expanded combined relative uncertainty                     |
|                |                                    | Greek Symbol   |
| $\epsilon$     |                                    | depth of pair potential                                    |
| $\kappa$       | J m <sup>5</sup> mol <sup>-2</sup> | influence parameter DGT                                    |
| $\mu$          | J mol <sup>-1</sup>                | chemical potential   |
| $\rho$         | mol m <sup>-3</sup>                | molar density  |
| $\sigma$       | Å                                  | segment diameter   |
| $\gamma$       | mN m <sup>-1</sup>                 | interfacial tension  |
| $\Delta\Omega$ | J mol <sup>-1</sup>                | grand thermodynamic potential                              |
|                |                                    | Abbreviation   |
| AAD            |                                    | average absolute deviation                                 |
| CP-PS-SAFT     |                                    | Critical Point-based Modified PC-SAFT                      |
| DGT            |                                    | density gradient theory                                    |
| EoS            |                                    | Equation of state  |
| GC-PPC-SAFT    |                                    | Group Contribution Polar PC-SAFT (GC-PPC-SAFT)             |
| LLE            |                                    | liquid-liquid equilibrium                                  |
| PC-SAFT        |                                    | Perturbed-Chain Statistical Associating Fluid Theory       |
| VLE            |                                    | vapor-liquid equilibrium                                   |
| VLE            |                                    | vapor-liquid-liquid equilibrium                            |
| PC-SAFT        |                                    | Perturbed Chain Polar Statistical Association Fluid Theory |
| Std.           |                                    | Standard deviation   |
| PD             |                                    | Pendant drop method  |
| DFT            |                                    | Density functional theory                                  |
| IFT            |                                    | Interfacial tension  |
| SRK            |                                    | Soave-Redlich-Kwong  |
| PRP            |                                    | Peng-Robinson  |
| BWR            |                                    | Benedict-Webb-Rubin  |
| CPA            |                                    | Cubic Plus Association                                     |

## References

- R. Villablanca-Ahues, R. Nagl, T. Zeiner, P. Jaeger, Interactions at the interfaces of the H<sub>2</sub>-brine-cement systems at elevated pressures for H<sub>2</sub> storage (doi), *Colloids Surf. A Physicochem Eng. Asp.* (2024), <https://doi.org/10.1016/j.colsurfa.2024.134091>.
- S. Mohammed, G.A. Mansoori, Molecular insights on the interfacial and transport properties of supercritical CO<sub>2</sub>/brine/crude oil ternary system, *J. Mol. Liq.* 263 (2018) 268–273.
- Samara, H., Von Ostrowski, T. & Jaeger, P. Geological Storage of Carbon Dioxide and Hydrogen in Jordanian Shale Formations. in *Proceedings - SPE Annual Technical Conference and Exhibition vols 2022-October (Society of Petroleum Engineers (SPE), 2022)*.
- A. Bahramian, A. Danesh, F. Gozalpour, B. Tohidi, A.C. Todd, Vapour-liquid interfacial tension of water and hydrocarbon mixture at high pressure and high temperature conditions. *Fluid Phase Equilib.* 252 (2007) 66–73.
- J. Nagarajan, M. Khaled, N.A. Gaseem, R.L. Robinson, Preprints of the 29th high pressure conference, *J. Chem. Eng. Data* vol. 35 (1990). (<https://pubs.acs.org/sharingguidelines>).
- M. Kodera, K. Watanabe, M. Lassiège, S. Alavi, R. Ohmura, Interfacial tension between decane saturated with methane and water from 283.2 K to 298.2 K under pressures upto 10 MPa. *J. Ind. Eng. Chem.* 81 (2020) 360–366.
- Monje-Galvan, V. & Klauda, J.B. Interfacial Properties of Aqueous Solutions of Butanol Isomers and Cyclohexane. (2020).
- S. Stephan, F. Fleckenstein, H. Hasse, Vapor-Liquid Interfacial Properties of the Systems (Toluene + CO<sub>2</sub>) and (Toluene + N<sub>2</sub>): Experiments, Molecular Simulation, and Density Gradient Theory, *J. Chem. Eng. Data* (2023), <https://doi.org/10.1021/acs.jced.3c00338>.
- S. Stephan, S. Becker, K. Langenbach, H. Hasse, Vapor-liquid interfacial properties of the system cyclohexane + CO<sub>2</sub>: Experiments, molecular simulation and density gradient theory, *Fluid Phase Equilib.* 518 (2020).
- F. Llovel, N. Mac Dowell, F.J. Blas, A. Galindo, G. Jackson, Application of the SAFT-VR density functional theory to the prediction of the interfacial properties of mixtures of relevance to reservoir engineering, *Fluid Phase Equilib.* 336 (2012) 137–150.
- T. Lafitte, B. Mendiboure, M.M. Piñero, D. Bessières, C. Miqueu, Interfacial properties of water/CO<sub>2</sub>: a comprehensive description through a gradient theory-SAFT-VR mie approach. *J. Phys. Chem. B* 114 (2010) 11110–11116.
- F. Biscay, A. Ghoufi, V. Lachet, P. Malfreyt, Monte Carlo calculation of the methane-water interfacial tension at high pressures, *J. Chem. Phys.* 131 (2009).
- G. Niño-Amézquita, D. van Putten, S. Enders, Phase equilibrium and interfacial properties of water+CO<sub>2</sub> mixtures, *Fluid Phase Equilib.* 332 (2012) 40–47.
- S. Enders, H. Kahl, Interfacial properties of water + alcohol mixtures, *Fluid Phase Equilib.* 263 (2008) 160–167.
- H. Kahl, S. Enders, Interfacial properties of binary mixtures, *Phys. Chem. Chem. Phys.* vol. 4 (2002) 931–936.
- A. Georgiadis, G. Maitland, J.P.M. Trusler, A. Bismarck, Interfacial tension measurements of the (H<sub>2</sub>O + n-decane + CO<sub>2</sub>) ternary system at elevated pressures and temperatures, *J. Chem. Eng. Data* 56 (2011) 4900–4908.
- F.D. Lenahan, Z. Zhai, C.J. Kankanamge, T. Klein, A.P. Fröba, Viscosity and interfacial tension of ternary mixtures consisting of linear alkanes, alcohols, and/or dissolved gases using surface light scattering and equilibrium molecular dynamics simulations, *Int J. Thermophys.* 43 (2022).
- T. Grunert, S. Enders, Prediction of interfacial properties of the ternary system water+benzene+butan-1-ol, *Fluid Phase Equilib.* 381 (2014) 46–50.
- R. Villablanca-Ahues, R. Nagl, T. Zeiner, P. Jaeger, Interfacial tension and phase equilibria for binary systems containing (CH<sub>4</sub>-CO<sub>2</sub>)+(n-dodecane; n-butanol; water), *Fluid Phase Equilib.* 570 (2023).
- O.G. Niño-Amézquita, S. Enders, Phase equilibrium and interfacial properties of water + methane mixtures, *Fluid Phase Equilib.* 407 (2016) 143–151.
- A. Georgiadis, et al., Interfacial tension measurements and modelling of (carbon dioxide + n-alkane) and (carbon dioxide + water) binary mixtures at elevated pressures and temperatures, *J. Supercrit. Fluids* 55 (2010) 743–754.
- O.G. Niño-Amézquita, S. Enders, P.T. Jaeger, R. Eggers, Interfacial properties of mixtures containing supercritical gases, *J. Supercrit. Fluids* 55 (2010) 724–734.
- O.G. Niño-Amézquita, S. Enders, P. Jaeger, R. Eggers, Measurement and Prediction of interfacial tension of binary mixtures, *Ind. Eng. Chem. Res* 49 (2010) 592–601.
- N. Choudhary, M.F.A. Che Ruslan, A.K. Narayanan Nair, S. Sun, Bulk and interfacial properties of alkanes in the presence of carbon dioxide, methane, and their mixture, *Ind. Eng. Chem. Res* 60 (2021) 729–738.
- B. Liu, et al., Reduction in interfacial tension of water-oil interface by supercritical CO<sub>2</sub> in enhanced oil recovery processes studied with molecular dynamics simulation, *J. Supercrit. Fluids* 111 (2016) 171–178.
- M. Cartes, G. Chaparro, A. Mejía, A novel experimental procedure to measure the bulk mass densities and interfacial tensions for mixtures at vapor-liquid-liquid equilibria, *J. Chem. Eng. Data* 65 (2020) 3344–3356.
- Stabinger, H. Density Measurement using modern oscillating transducers. *South Yorkshire Trading Standards Unit* (1994).
- Taylor, B.N. & Kuyatt, C.E. Guidelines for Evaluating and Expressing the Uncertainty of NIST Measurement Results. (1994).
- S. Knauer, M.R. Schenk, T. Köddermann, D. Reith, P. Jaeger, Interfacial tension and related properties of ionic liquids in CH<sub>4</sub> and CO<sub>2</sub> at elevated pressures: experimental data and molecular dynamics simulation, *J. Chem. Eng. Data* 62 (2017) 2234–2243.
- B. Song, J. Springer, Determination of interfacial tension from the profile of a pendant drop using computer-aided image processing, *J. Colloid Interface Sci.* 184 (1996) 64–76.
- A. Hebach, et al., Interfacial tension at elevated pressures-measurements and correlations in the water + carbon dioxide system, *J. Chem. Eng. Data* 47 (2002) 1540–1546.
- Y. Sutjiadi-Sia, H. Marckmann, R. Eggers, C. Holzknicht, S. Kabelac, Zum Einfluss von in Flüssigkeiten Unter Druck Gelösten Gasen auf Grenzflächenspannungen und Benetzungseigenschaften. *Forsch. Im. Ing. /Eng. Res.* 71 (2007) 29–45.
- S. Zepieri, J. Rodríguez, A.L. López De Ramos, Interfacial tension of alkane + water systems, *J. Chem. Eng. Data* 46 (2001) 1086–1088.
- A. Goebel, K. Lunkenheimer, Interfacial tension of the water/n-alkane interface, *Langmuir* 13 (1997) 369–372.
- J.D. Berry, M.J. Neeson, R.R. Dagastine, D.Y.C. Chan, R.F. Tabor, Measurement of surface and interfacial tension using pendant drop tensiometry, *J. Colloid Interface Sci.* 454 (2015) 226–237.
- A.M. Worthington, IV. Note on a point in the theory of pendent drops, *London, Dublin Philos. Mag. J. Sci.* 19 (1885) 46–48.
- D. Villers, J.K. Platten, Temperature dependence of the interfacial tension between water and long-chain alcohols, *J. Phys. Chem.* 92 (1988) 4023–4024.
- J. Gross, G. Sadowski, Application of the perturbed-chain saft equation of state to associating systems, *Ind. Chem. Eng. Res.* 41 (2001) 5510–5515.
- J. Gross, J. Vrabec, An equation-of-state contribution for polar components: dipolar molecules, *AIChE J.* 52 (2006) 1194–1204.
- J. Gross, G. Sadowski, Perturbed-chain SAFT: an equation of state based on a perturbation theory for chain molecules, *Ind. Eng. Chem. Res* 40 (2001) 1244–1260.
- J. Gross, An equation-of-state contribution for polar components: Quadrupolar molecules, *AIChE J.* vol. 51 (2005) 2556–2568.
- J.W. Cahn, J.E. Hilliard, Free energy of a nonuniform system. i. interfacial free energy, *J. Chem. Phys.* 28 (1958) 258–267.
- C.I. Poser, I.C. Sanchez, Interfacial tension theory of low and high molecular weight liquid mixtures, *Am. Chem. Soc.* 14 (1981) 361–370.

- [44] S. Enders, K. Quitzsch, Calculation of interfacial properties of demixed fluids using density gradient theory, *Langmuir* 14 (1998) 4606–4614.
- [45] R. Evans, The nature of the liquid-vapour interface and other topics in the statistical mechanics of non-uniform, classical fluids, *Adv. Phys.* 28 (1979) 143–200.
- [46] R. Nagl, P. Zimmermann, T. Zeiner, Interfacial mass transfer in water–toluene systems, *J. Chem. Eng. Data* 65 (2020) 328–336.
- [47] R. Nagl, T. Zeiner, P. Zimmermann, Interfacial mass transfer in quaternary liquid-liquid systems, *Chem. Eng. Process. - Process. Intensif.* 171 (2022) 108501.
- [48] O.G. Nino-Amezquita, S. Enders, P.T. Jaeger, R. Eggers, Measurement and prediction of interfacial tension of binary mixtures, *Ind. Eng. Chem. Res* 49 (2010) 592–601.
- [49] O.G. Enders, S. Prediction of interfacial tension of binary mixtures, *Nino-Am. ézquita* (2010) 85–90, [https://doi.org/10.1016/S1570-7946\(10\)28015-X](https://doi.org/10.1016/S1570-7946(10)28015-X).
- [50] E. Schäfer, G. Sadowski, S. Enders, Interfacial tension of binary mixtures exhibiting azeotropic behavior: measurement and modeling with PCP-SAFT combined with density gradient theory, *Fluid Phase Equilib.* 362 (2014) 151–162.
- [51] N. Haarmann, A. Reinhardt, A. Danzer, G. Sadowski, S. Enders, Modeling of interfacial tensions of long-chain molecules and related mixtures using perturbed chain-statistical associating fluid theory and the density gradient theory, *J. Chem. Eng. Data* 65 (2020) 1005–1018.
- [52] C. Bühl, S. Enders, Prediction of interfacial properties of ternary, sulfur-containing mixtures, *J. Chem. Eng. Data* 61 (2016) 4261–4269.
- [53] T. Grunert, H. Rudolph, S. Enders, Prediction of interfacial tensions between demixed ternary mixtures, *Z. F. ür. Phys. Chem.* 227 (2013) 269–284.
- [54] A. Danzer, S. Enders, Theoretical and experimental investigation of the interfacial properties in the ternary mixtures water + 1-hexanol + acetic acid and water + hexylacetate + acetic acid using density gradient theory and spinning-drop tensiometry, *J. Mol. Liq.* 283 (2019) 482–490.
- [55] T. Goetsch, et al., Liquid–Liquid equilibrium and interfacial tension of hexane isomers–methanol systems, *Ind. Eng. Chem. Res* 56 (2017) 9743–9752.
- [56] A.K. Chicaroux, T. Zeiner, Investigation of interfacial properties of aqueous two-phase systems by density gradient theory, *Fluid Phase Equilib.* 407 (2016) 135–142.
- [57] H.I. Chen, H.Y. Chang, P.H. Chen, High-pressure phase equilibria of carbon dioxide + 1-butanol, and carbon dioxide + water + 1-butanol systems, *J. Chem. Eng. Data* 47 (2002) 776–780.
- [58] Z. Duan, J. Hu, D. Li, S. Mao, Densities of the CO<sub>2</sub>-H<sub>2</sub>O and CO<sub>2</sub>-H<sub>2</sub>O-NaCl systems up to 647 K and 100 MPa, *Energy Fuels* 22 (2008) 1666–1674.
- [59] Z. Pan, J.P.M. Trusler, Experimental and modelling study of the interfacial tension of (n-decane + carbon dioxide + water) in the three phase region, *Fluid Phase Equilib.* 568 (2023).
- [60] N. Choudhary, A.K. Narayanan Nair, M.F.A. Che Ruslan, S. Sun, Bulk and interfacial properties of decane in the presence of carbon dioxide, methane, and their mixture, *Sci. Rep.* 9 (2019).
- [61] R. Nagl, S. Stocker, P. Zimmermann, T. Zeiner, Study on mass transfer in reactive liquid-liquid systems, *Chem. Eng. Res. Des.* 186 (2022) 541–555.
- [62] M.P.W.M. Rijkers, V.B. Maduro, C.J. Peters, J. De, S. Arons, Measurements on the phase behavior of binary mixtures for modeling the condensation behavior of natural gas part II. the system methane + dodecane, *Fluid Phase Equilibria* vol. 72 (1992).